nature portfolio

Peer Review File

Machine learning-assisted dual-atom sites design with interpretable descriptors unifying electrocatalytic reactions

REVIEWER COMMENTS

Reviewer #1 (Remarks to the Author):

This paper describes a new descriptor that relates to multiple different reactions. The authors report that by using this new descriptor (ARSC) they were able to predict an optimal bifunctional ORR/OER electrocatalyst. Overall, it is interesting to have a new descriptor. However, one of the main problems I see, is that most of these materials are not the same material during all these reactions, which means that the sites being calculated for ORR are not the same sites that should be examined for OER. This change in material would need to be addressed both in the model and in the electrochemical verification.

In terms of EXAFS analysis of the SACs, please be aware of the limits of detection for single atoms via EXAFS: https://pubs.acs.org/doi/full/10.1021/acscatal.3c01116 and update the discussion accordingly.

Based on thermodynamics (see Pourbaix diagrams), most of these electrocatalysts would not be the same material for OER and ORR, for example. During OER specifically, most of these active sites would degrade: https://pubs.acs.org/doi/10.1021/acsenergylett.8b01774 . This means, that while it is interesting that there is a correlation between the descriptor and performance, it is confusing how this would be possible if the material is not in situ the same material as what is being used to inform the descriptor that relies on pristine: X-X-C and X-X-NO sites, which are likely not stable during OER. To have something that is more realistically useful, it would be necessary to incorporate a Pourbaix diagram / stability analysis for the most stable binding surface then use that surface in the analysis. Alternatively, the authors could show experimentally that these are the most stable surfaces for all reactions tested, but based on the extensive carbon corrosion seen during OER, this seems unlikely.

Reviewer #2 (Remarks to the Author):

Dual-atom catalysts, possessing the synergistic effects between the two atoms, have increasingly garnered attention due to their unique, tunable chemical and physical properties, as well as their catalytic performance. One significant challenge in designing DAC through a bottom-up approach lies in the immense variety of atomic parings, support choices, and coordination environment changes. This complexity greatly limits the feasibility of direct density functional theory (DFT) calculations which requires substantial computational resources.
In this work, Lin et al. introduce an Interpretable machine learning approach (ARSC) to conduct high-throughput catalyst screening, incorporating the atomic property (A), reactant (R), synergistic (S), and coordination effects (C). Starting from the physical foundation of the d-band theory, they propose a primitive descriptor considering the d-band filling (fd) and width (Wd) from three electrocatalysis reactions (ORR/OER, CRR, and NRR) over homonuclear DACs, followed by the transformation to the physical properties of the elements that closely related to the fd and wd. Moving forward, the descriptor is refined i) based on the reaction types through the feature engineering approach and ii) by considering

the coordination effects. In the end, the well-developed descriptor is applied for catalyst screening and the prediction is validated through experimental effort.

Overall, by leveraging the DFT calculations and ML approach, this work introduces a simple well-refined descriptor, achieves the high throughout catalyst screening, and conducts the experimental validation. It is an interesting, timely, and well-ordered work regarding the rising attention towards the DACs in catalysis and the application of Machine learning in catalyst screen and design. However, to the best of my knowledge, there are several comments that should be addressed to deepen the understanding and enhance the overall quality of this work prior to publication.

Comment #1. The physical basis of this work is the d-band theory which is typically applied to the heterogeneous system such as metal surfaces and nanoparticles. However, SAC and DAC resemble homogeneous systems and demonstrates the molecular complex characteristics, it is questionable to apply the d-orbital theory for DACs. Recent works on SAC demonstrates that the frontier orbitals play the essential role in determining the interactions between species and the catalyst, as evidenced by publications in PRL, 2020, 125, 156001, ACS Catal. 2024, 14, 2, 886–896, and Angew. Chem. Int. Ed. 2024, 63, e202311174. Given that i) some of the d-orbitals participate in forming bonds with the supports and ii) the frontier orbitals mostly contribute to the adsorbate bindings. Shifting the d-band theory (which containing all d-orbitals) to the specific frontier d-orbitals (main contributor to the adsorptions) could offer deeper physical insight and aid in developing more accurate descriptors for DACs.

Comment #2. Beyond the extensive combinations of X-Y that limits the DFT efforts for searching the optima catalysts, the stability of DACs presents as another crucial criterion for catalyst screening. In the context of the 840 DACs, assessing their stability becomes imperative. How should their stability be evaluated? If the catalyst is highly unstable, what is the meaning to conduct DFT calculations?

Comment #3. In Section , the author mentioned that “Wd is solely influenced by the d-orbital size, presenting as a negative function of atomic radius (R) and the number of electron shells (S) ($Wd \propto 1/(R \times S)$)”. However, the description of the atomic radius is ambiguous. There are several types of atomic radius using in chemistry. It can be inferred from the values that “R” is the atomic radii computed from theoretical models by Enrico Clement (J. Chem. Phys. 47, 1300–1307 (1967). As metal atom binds to N and possesses positive charges, why not using Ionic radius? In addition, what are the behaviors of metallic radius and covalent radius?

Comment #4 In figure 2e and other figures related to linear scaling relations (LSRs), the broad energy span and large dataset facilitate achieving an ideal R2 value effortlessly. It is recommended that the authors to thoroughly evaluate the LSRs by including more regression results such as mean absolute error, maximum positive/negative error and root mean square errors.

Comment #5: It is common that there is a tradeoff between the computational dataset size and the accuracy. Guaranteeing the quality of the input dataset is vital for the effective training ML models and generating predictions with physical meanings. Specifically, for DACs containing elements like Fe, Co, and Ni, it is important to detail how the accuracy of electronic states' (doublet, triplet, etc.) collection is ensured.

Comment #6 While this work leverages descriptors and machine learning for catalyst screening, leading to the prediction and experimental validation of Co-Co/Ir-Qv3 as an optimal oxygen electrocatalyst due to its moderate ARSC value. Compared to the extensive efforts in database creation (840 catalysts), it raises the question of why further DFT analysis on this specific DAC wasn't conducted. I believe that further DFT investigations on Co-Co/Ir-Qv3 could significantly aid in uncovering its unique features that lead to superior catalytic efficiency. Such analyses would offer deeper atomic-level insights into what

constitutes an "ideal" catalyst.
Comment #7 In the end of the results, the authors discussed the model's adaptability to different supports by altering the coordination from N to C and O for X-X type catalysts. While promising linear scaling relations (LSRs) are noted for OER and CRR, the model's applicability appears compromised for NRR over X-Y type catalysts, as evidenced by deteriorating scaling and notable outliers in Fig. S31 (R2 is also missing), indicating the model's limitations in more complex coordination environments. Therefore, it's crucial that the authors address the potential limitations, shortcomings, or areas for refinement when applying their approach to more intricate DACs that utilize non-uniform supports, with a few sentences in the conclusion.
Comment #9:
I highly recommend incorporating a comprehensive workflow diagram detailing the entire project, which should cover dataset construction, descriptor refinement, ML prediction, and experimental validation processes. Additionally, including a table that lists all symbols used along with their physical meanings would greatly enhance the manuscript's readability. Also, it is weird to plot the volcano curve with a V-shape by using “-UL” in Fig. S1 and S2.
Comment #10:
Throughout the manuscript and SI, there's a noticeable absence of detailed descriptions regarding the DFT models, aside from the simplified local configurations depicted in figures and a brief mention of using a monolayer graphene as the support. Moreover, the Python codes utilized in the analysis have not been shared. This omission makes it almost impossible to ensure the reproducibility of this work. To address this issue and support the growing DAC community, particularly those focused on electrocatalytic reactions, and to keep with the journal’s open-source ethos, it is strongly recommended/encouraged that the configurations be provided in commonly used formats such as VASP (POSCAR, CONTCAR) or extended XYZ. These files should be zipped and included as supporting information and the Python codes should be uploaded to platforms like GitHub. Making these details resources readily accessible, rather than “upon request”, ensures that other researchers can replicate the study's findings and apply the configurations to their own work, fostering further advancements in this field.

Reviewer #3 (Remarks to the Author):

In this paper, X. Lin et al. presents a novel interpretable descriptor model, called ARSC, which integrates activity and selectivity prediction across multiple electrocatalytic reactions (such as O2/CO2/N2 reduction and O2 evolution reactions). ARSC relies solely on easily accessible intrinsic properties and effectively disentangles atomic properties, reactants, synergistic effects, and coordination influences on the d-band shape of dual-atom sites. It is developed through a physically meaningful feature engineering and selection/sparsification (PFESS) method. By leveraging ARSC, optimal catalysts for various products can be rapidly identified without resorting to over 50,000 density functional theory calculations. The universality of the model is confirmed through extensive validation against existing literature and subsequent experiments, which pinpoint Co-Co/Ir-Qv3 as top bifunctional oxygen reduction and evolution electrocatalysts.
Unfortunately, I have several critical concerns, which should be properly clarified before I agree to the

publication of this manuscript:

1. While the target catalyst or products may differ from those in previous reports, it's worth noting that descriptor-based approaches have been published several times before. Could you please discuss these papers and the differences with them?

a) Nat. Commun. 14, 4449 (2023)
b) Nat. Nanotech. 17, 606–612 (2022)
c) J. Mater. Chem. A,10, 1451-1462 (2022)
d) Nat. Commun. 12, 1833 (2021)
e) J. Phys. Chem. Lett. 11, 3481–3487 (2020)

2. I believe that the efficiency of the catalyst is not significantly superior compared to other catalysts, and it is important to provide more detailed information. As the author suggested in Supplementary Table 11, various previous ORR catalysts are listed. However, the level of detail provided is not sufficient for a reasonable comparison. The concentration of electrolyte, pH, substrate, and other relevant parameters should be tabulated and compared with other catalysts.

3. For reproducibility, the error bars should be accurately expressed in the data, including overpotential.

4. One of the key factors to consider is the degradation of catalysts. Although the overpotential is much lower, if the duration is not sufficient, the catalyst may be difficult to consider as a superior catalyst. Could you please suggest including cycling or duration data in detail and comparing it to other reported catalysts?

5. The author primarily focused on suggesting the thermodynamic overpotential without addressing kinetics, except for the experimental Tafel plot in Supplementary Fig. 27. It would be beneficial to include kinetics barriers by employing (CI)-NEB methods.

6. Nowadays, new pathways for the oxygen reduction reaction (ORR) have been suggested, unlike the conventional one (O2 -> OOH -> O -> OH). If you apply a new pathway, are you confident that this trend can be maintained?

7. How can the solvation effect be included? If I haven't missed any information regarding this, there doesn't seem to be any discussion about the solvation effect. Could you please suggest the results when you include the solvation effect?

8. Previous high-throughput studies have already covered Co-Co dual atom catalysts. Could you please carefully compare your results with those of other studies? If there are discrepancies, kindly discuss the reasons for the differences.

9. If I understand correctly, there are some ad hoc or artificial parameters. For examples, the coefficient of alpha (k) is defined as one without any justification I wonder whether is there any physical or chemical reason to set this parameter like this or just numerically fit?

10. Compared to other descriptors reported previously, how much superior are yours? For example, consider using other descriptors to extract candidates, synthesize and characterize them, and evaluate their electrochemical performance. Finally, compare the catalytic activity of your candidates with those obtained using other descriptors.

As a final comment, for the benefit of the data-driven society, I would suggest sharing the raw data and machine learning model on platforms like GitHub or Zendo. However, if you believe this information needs to remain confidential during the review or revision process, I recommend releasing the raw data and model after acceptance or publication.

Reviewer #4 (Remarks to the Author):

I co-reviewed this manuscript with one of the reviewers who provided the listed reports. This is part of the Nature Communications initiative to facilitate training in peer review and to provide appropriate recognition for Early Career Researchers who co-review manuscripts.

Reviewer #1:

General Comments R1: *This paper describes a new descriptor that relates to multiple different reactions. The authors report that by using this new descriptor (ARSC) they were able to predict an optimal bifunctional ORR/OER electrocatalyst. Overall, it is interesting to have a new descriptor. However, one of the main problems I see, is that most of these materials are not the same material during all these reactions, which means that the sites being calculated for ORR are not the same sites that should be examined for OER. This change in material would need to be addressed both in the model and in the electrochemical verification.*

Response: We are very grateful to the reviewer for the careful review of our work. The constructive suggestions are very helpful in improving the quality of this work. We are especially grateful for the opportunity to address these questions. We have seriously considered your comments and supplemented the related descriptions and improved our manuscript based on each of the points you have made. By combining the Pourbaix diagram and stability analysis, we have re-identified the real active sites in DACs during OER and verified that our descriptor ARSC can still describe OER activities on DACs when k = 0.05. It is worth noting that Co-Co/Ir-Qv3 exhibit the lower U_L(OER) when we considered the real active sites instead of the pristine one, in better agreement with our experimental results. Corresponding details are listed in R1-2.

Specific Comment R1-1: *In terms of EXAFS analysis of the SACs, please be aware of the limits of detection for single atoms via EXAFS : https://pubs.acs.org/doi/full/10.1021/acscatal.3c01116 and update the discussion accordingly.*

Response: We thank the reviewer for this important comment very much. According to this valuable paper the reviewer mentioned, to exclude the possibility of metallic and oxidized clusters, it is necessary to fit EXAFS beyond the first shell and consider multiple structural models (**S. R. Bare** et al., *ACS Catal.* 2023, 13, 6462−6473). Therefore, we re-analyzed the EXAFS data, including 3 scattering paths for Co-Co-Qv3 models and 2 scattering paths for metallic or oxidized Co models, as shown in **Supplementary Table 13 and Supplementary Fig. 41**. The results reveal that the Co-Co-Qv3 model exhibit the best fitting results compared to Co_3O_4, metallic Co, or the mixed structural models, suggesting that the structure of the Co-Co-NC sample are more likely to be Co-Co-Qv3. Firstly, to investigate whether the Co-Co-NC sample contain partial oxide clusters, we found that the best fitting occurs when the coordination numbers of Co-Co path were constrained to 1 for oxidized Co as structural models. However, its goodness of fit is far inferior to that of Co-Co-Qv3 (fitting 2). When we used Co-Co-NC instead of oxidized Co to fit the first shell, there is some improvement in the overall fitting effect (fitting 3); however, it still lags significantly behind the performance of Co-Co-NC alone due to the poor fitting at the second shell. All these results suggest the absence of oxidized Co clusters. Secondly,

for metallic clusters, one can see that that the Co-Co path in metallic Co fail to fit the data well, with its R-factor being as high as 0.108 at the lowest, indicating the absence of metallic Co clusters (fitting 4). It also demonstrates the non-bonded local structure of Co-Co in Co-Co-NC, in line with our expectations. We also re-fitted the EXAFS data for Co-Ir-NC and obtained the same results (**Supplementary Table 14**). **In conclusion, our as-synthesized Co-Co/Ir-NC samples more likely to have specific local structures of Co-Co/Ir-Qv3 rather than metallic or oxidized clusters.** In addition, for a more rigorous argument, we cited the relevant paper (**S. R. Bare** et al., *ACS Catal.* 2023, 13, 6462−6473) to let readers know the potential limits of detection for single atoms via EXAFS in our manuscript.

We have updated the statement in the manuscript *page 16*:

It is worth noting that simply fitting the first shell alone is not effective in distinguishing between single atoms or metallic/oxidized clusters[41]. The EXAFS fitting for 3 scattering paths and comparisons between multiple structural models imply the absence of clusters and the non-bonded local structure of metal-metal in Co-Co/Ir-NC (**Supplementary Fig. 41 and Supplementary Tables 13 and 14**).

41. Finzel, J. et al. Limits of detection for EXAFS characterization of heterogeneous single-atom catalysts. *ACS Catal.* **13**, 6462-6473 (2023).

We have updated the **Supplementary Tables 13 and 14** in the Supplementary Information:

Supplementary Table 13. EXAFS fit parameters for Co-Co-NC with different structural models.

Fitting	Structural model	Path	*CN*	*R* (Å)	$\sigma^2\times10^2$ (Å^2)	ΔE_0 (eV)	R factor
1	Co-Co-Qv3	Co-N	4.5±0.3	2.07±0.01	0.6±0.1	4.2±0.4	0.018
		Co-C	3.2±0.6	2.79±0.02	0.5±0.2		
		Co-C	3.9±0.5	3.09±0.01	0.3±0.2		
2	Co_3O_4	Co-O	4.3±1.0	2.03±0.01	1.0±0.3	-3.2±1.2	0.053
		Co-Co	1[a]	3.05±0.04	0.8±0.4		
3	Co-Co-Qv3	Co-N	4.9±0.3	2.05±0.01	1.0±0.1	-0.7±1.6	0.045
	Co_3O_4	Co-Co	1[a]	3.07±0.03	0.7±0.3	-1.4±0.4	
4	Co-Co-Qv3	Co-N	4.3±0.9	2.05±0.01	0.8±0.4	-1.2±0.2	0.108
	Metallic Co	Co-Co	1[a]	2.52±0.03	1.0[b]	-0.4±0.1	

S_0^2: amplitude reduction factor, which is fixed as 0.97 for Co based on fitting of the metal standard; *CN*: coordination numbers; *R*: bond distance; σ^2: Debye-Waller factors; ΔE_0: the inner potential correction. *R* factor is used to value the goodness of fit. Data ranges: 3.0 ≤ *k* ≤ 13.0 Å^{-1}, 1.0 ≤ R ≤ 3.0 Å.
[a]These *CN*(Co-Co) were constrained to above 1 in metallic Co clusters or oxidized Co clusters to obtain the best fitting results within the reasonable parameters. This setting is according to the rule that the lowest *CN*(Co-Co) is 1 in metallic Co clusters or oxidized Co clusters.
[b]σ^2 was constrained to below 1.0 × 10^{-2} Å^2 to obtain the best fitting results within the reasonable parameters.

Supplementary Table 14. EXAFS fit parameters for Co-Co-NC and Co-Ir-NC.

Sample	Path	*CN*	*R* (Å)	σ^2×10^2 (Å^2)	ΔE_0 (eV)
	Co-N	4.5±0.3	2.07±0.01	0.6±0.1	
Co-Co-NC	Co-C	3.2±0.6	2.79±0.02	0.5±0.2	4.2±0.4
	Co-C	3.9±0.5	3.09±0.01	0.3±0.2	
	Co-N	4.4±0.6	2.07±0.02	0.5±0.2	
Co-Ir-NC	Co-C	2.1±1.3	2.78±0.03	0.6±0.1	3.8±0.8
	Co-C	3.8±1.2	3.07±0.02	0.5±0.2	
	Ir-N	4.3±0.3	2.01±0.01	0.6±0.1	
Co-Ir-NC	Ir-C	1.5±0.6	2.69±0.01	0.8±0.3	-0.9±0.2
	Ir-C	1.1±0.5	3.16±0.03	1.0±0.4	

S_0^2: amplitude reduction factor, which is fixed as 0.97/0.89 for Co/Ir based on fitting of the metal standard, respectively; *CN*: coordination numbers; *R*: bond distance; σ^2: Debye-Waller factors; ΔE_0: the inner potential correction. *R* factor is used to value the goodness of fit, which is < 0.02 in this work. Data ranges: 3.0 ≤ *k* ≤ 13.0 Å^{-1}, 1.0 ≤ R ≤ 3.0 Å. The best fitting model for the sample Co-Co-NC and Co-Ir-NC is Co-Co-Qv3 and Co-Ir-Qv3, respectively.

We have provided the **Supplementary Fig. 41** in the Supplementary Information:

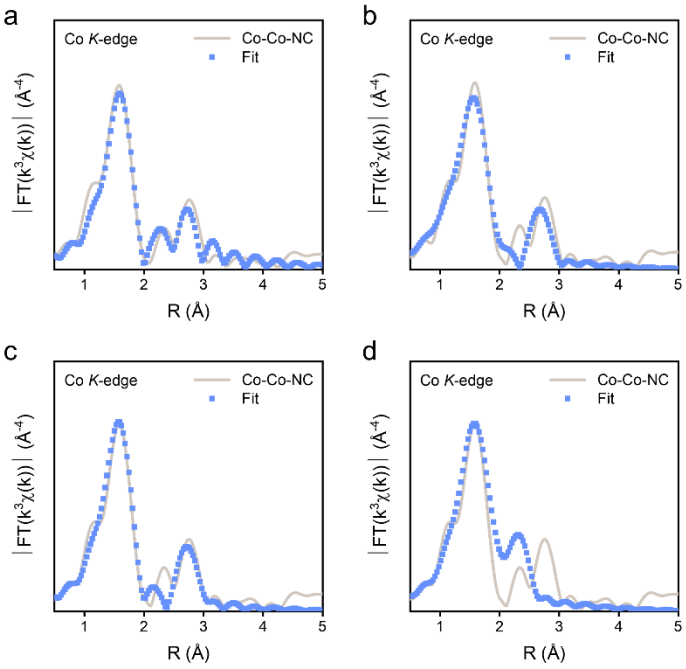

Supplementary Fig. 41. Co *K*-edge EXAFS fitting curves in R space for **a** fitting 1, **b** fitting 2, **c** fitting 3, and **d** fitting 4. The data are k^3-weighted and not phase-corrected.

Specific Comment R1-2: *Based on thermodynamics (see Pourbaix diagrams), most of these electrocatalysts would not be the same material for OER and ORR, for example. During OER specifically, most of these active sites would degrade: https://pubs.acs.org/doi/10.1021/acsenergylett.8b01774 . This means, that while it is interesting that there is a correlation between the descriptor and performance, it is confusing how this would be possible if the material is not in situ the same material as what is being used to inform the descriptor that relies on pristine: X-X-C and X-X-NO sites, which are likely not stable during OER. To have something that is more realistically useful, it would be necessary to incorporate a Pourbaix diagram / stability analysis for the most stable binding surface then use that surface in the analysis. Alternatively, the authors could show experimentally that these are the most stable surfaces for all reactions tested, but based on the extensive carbon corrosion seen during OER, this seems unlikely.*

Response: We are very grateful to the reviewers for your helpful comments, which we really did not consider in previous submission. We fully agree that due to the oxidation and degradation of active sites during OER widely reported by previous works (**C. B. Mullins** et al., *ACS Energy Lett.* 2018, 3, 2956−2966), a pristine dual-atom sites serving as the active site for ORR may no longer be suitable for the OER. It means that it becomes questionable whether our proposed descriptor ARSC can also describe the structure-activity relationship of DACs under the real OER condition. To clarify this issue, we first investigated the real active sites of DACs during OER by plotting the Pourbaix diagrams. Then, we re-calculated the OER activity of all DACs mentioned in **Fig.5b** and revised the descriptor ARSC to reflect the structure-

performance relationship of DACs under OER conditions. In addition, given the issue of catalyst durability in OER, we also evaluated the stability of DACs both computationally and experimentally. **Using Pourbaix diagrams, we have identified the real active sites in OER condition, which is covered by *O for most DACs. At the same time, we have verified that those active sites have great potential to be stable during OER, especially for our identified high-efficiency Co-Co/Ir-Qv3 catalysts. All these results suggest the universality of our proposed descriptor ARSC for not only the pristine surfaces but also the real active sites during OER.**

To identify the surface state of DACs under OER conditions, we calculated the adsorption free energies of *O, *OH, *O + *OH, *OH + *OH, and *O + *O with all possible adsorption configurations, as shown in **Supplementary Fig. 26**. The *O and *OH are adsorbed on the metal atoms much more strongly than on C or N atoms of the substrate, suggesting that the metal centers of DACs are the real reaction sites for ORR/OER. Taking Co-Co/Ir-Qv3, which is screened as the promising candidate for OER in our previous submission, as an example, their surface Pourbaix diagrams as the function of both potential and pH reveal that the active sites will be covered by the *O + *O state under the OER condition, while the pristine dual-atom site is more favorable under the ORR condition (**Supplementary Fig. 27**). This result suggests that the active sites of DACs are easily oxidized during OER, and these oxidized metal centers are the real active sites, in line with previous works (**H. Li** et al., *Commun. Chem.* 2023, 6, 6). Previous works has reported that for the *O-covered metal centers in metal-doped graphene-based systems, *O is more likely to participate in OER (**K. S. Kim** et al., *Energy Environ. Sci.* 2021, 14, 3455–3468). As a result, OER prefer to occur along Path-II on *O-covered DACs rather than Path-I on pristine DACs (**Supplementary Fig. 28**). As shown in **Supplementary Fig. 29**, U_L(OER) calculated via Path-II of Co-Co-Qv3 is 1.52 V, which is closer to our experimental results than that via Path-I (1.63 V). It further demonstrates the reliability of our calculations.

In addition to Co-Co/Ir-Qv3, we have summarized the surface states of DACs under OER conditions via Pourbaix diagrams, which is listed in **Supplementary Table 11**. The results show that all the main X-metals of DACs will be oxidized during OER. *O + *O is the most stable surface state for most DACs, which occupies all X-Y-Qv1 sites due to the stronger *O-binding of Qv1. Since Pd and Pt bind *O more weakly than other elements, these sites may be exposed during OER. For DACs with *O state, Path-I is favorable due to the lack of adsorbed *O on the Y-metal, and the *O adsorbed on the X-metal will participate in OER. While DACs with *OH + *O state prefer Path-III (**Supplementary Fig. 28**). Based on the real active sites we identified, the U_L(OER) of DACs have been re-calculated. More importantly, in line with other reactions, we find that the descriptor ARSC can also present a volcano-like correlation with OER activities for DACs with the *O-covered active sites when k = 0.05 (**Supplementary Fig. 30**). It is worth noting that k represents the weight of the coordination effect, and a larger k indicates that the reaction is more sensitive to the coordination structures of DACs. For ORR, k is 1, suggesting that the oxidation of the

active sites reduces the difference in OER activity between different coordination structures of DACs.

The reason why the descriptor ARSC is also applicable for describing OER activity can be well explained as follows. For active sites of DACs during OER, oxidized by *O is equal to O-coordination. We all known that ARSC include the atomic property, synergistic, and coordination effects of dual-atom sites simultaneously. The introduction of *O-species will not change the atomic property and synergistic effects of dual-atom sites, since they only depend on the intrinsic properties of metal atoms and metal-metal interactions, respectively. Only the coordination effects will be changed due to the oxidation of DACs. During OER, the activity of the metal centers is not just determined by the coordination atoms in the substrate anyone. Since most dual-atom sites with different coordination configurations are coordinated with the same *O-species at the same time during OER, the introduction of O-coordination will hinder the overall coordination effect governed by the difference of the N-coordination structures in the substrate.

Based on our comprehensive re-calculations for OER activity with the real active sites determined by Pourbaix diagrams, some candidates with promising OER activity are identified, such as Co-Co-Qv3, Co-Ir-Qv3, Co-Ni-Qv1, Co-Pt-Qv3, Co-Pd-Qv3 with U_L(OER) of 1.52, 1.52, 1.53, 1.55, 1.56 V, respectively. Among them, some DACs can serve as promising bifunctional oxygen electrocatalysts, such as Co-Co-Qv3 and Co-Ir-Qv3, but the other can only catalyze OER effectively, such as Co-Ni-Qv1. **It is worth noting that Co-Co-Qv3 and Co-Ir-Qv3 exhibit outstanding OER activities when we considered the real active sites instead of the pristine one, in better agreement with our experimental results.**

Furthermore, inspired by the kind reminder of the reviewer, the durability of 840 DACs has been also evaluated. The effective OER electrocatalysts with high stability have been widely reported in metal-doped carbon-based systems (**L. Liu** et al., *ACS Catal.* 2022, 12, 9397−9409), suggesting the potential for high stability of DACs we considered in this work. The stability analysis was conducted including the thermodynamic and electrochemical stability. This method is widely used in the stability assessment of metal-doped graphene-derived materials for OER, and its reliability and feasibility have been confirmed by many experimental and computational studies (**X. Sun** et al., *Nat. Commun.* 2023, 14, 4449; **K. S. Kim** et al., *Energy Environ. Sci.* 2021, 14, 3455–3468).

The stability over metal-aggregation is governed by the aggregation energy (E_{agg}), which is defined as:

$$E_{agg} = (E(X\text{-}Y\text{-}NC) - E(NC) - \mu(X) - \mu(Y)) / 2$$

where E(X-Y-NC) and E(NC) represent total energies of DACs and the defected nitrogenated graphene surface, respectively; μ(X) and μ(Y) are the energies of X-metal and Y-metal, which are taken from the bulk metals. The negative E_{agg} value indicates that the embedding into graphene is preferred over metal clustering. The E_{agg}

values for all 840 DACs are summarized in **Supplementary Fig. 31**. The results show that X-Y-Qv2 and X-Y-Qv3 are slightly more stable against clustering than X-Y-Qv4 and notably more stable than X-Y-Qv1. The majority of X-Y-Qv2 and X-Y-Qv3 sites exhibit sufficiently negative E_{agg}, suggesting the strong interaction between the dispersed X-Y sites and the coordination N atoms.

Furthermore, we utilized dissolution potential (U_{diss}) to determine the electrochemical stability against dissolution of X-Y sites (**J. K. Nørskov** et al., *Electrochim. Acta* 2007, 52, 5829–5836), which is defined as:

$$U_{diss}(X) = U^{o}_{diss}(X) - (E(X\text{-}Y\text{-}NC) - E(Y\text{-}NC) - \mu(X)) / en_e$$

$$U_{diss}(Y) = U^{o}_{diss}(Y) - (E(X\text{-}Y\text{-}NC) - E(X\text{-}NC) - \mu(Y)) / en_e$$

$$U_{diss} = \min[U_{diss}(X), U_{diss}(Y)]$$

where $U^{o}_{diss}(X)$ and $U^{o}_{diss}(Y)$ are the standard dissolution potential of bulk X-metal and Y-metal; n_e represent the number of transferred electrons involved in the dissolution; e is the electron charge; E(Y-NC) and E(X-NC) are the total energies of DACs with the vacancy of X-metal and Y-metal, respectively. The positive value of U_{diss} indicates that the dissolution of metal atoms can be better avoided under electrochemical reactions. As shown in **Supplementary Fig. 32**, X-Y-Qv2 and X-Y-Qv3 sites is more likely to maintain durability in a harsh electrochemical environment.

The stability of 840 DACs was comprehensively evaluated by plotting E_{agg} versus U_{diss} (**Supplementary Fig. 33**). We used $E_{agg} < 0$ eV and $U_{diss} > 0$ V as the standard for the unaggregatable and indissoluble system (**X. Sun** et al., *Nat. Commun.* 2023, 14, 4449; **K. S. Kim** et al., *Energy Environ. Sci.* 2021, 14, 3455–3468). The more negative the E_{agg} value and the more positive the U_{diss} value, the stronger the stability of DACs. It is found that the majority of X-Y-Qv2 and X-Y-Qv3 sites exhibit remarkable stability, while the metal atoms tend to aggregate and dissolve in the electrolyte in some X-Y-Qv4 and X-Y-Qv1 sites. Our calculations show that Fe, Co, Ni, Ru, Rh, Os, Ir-based DACs have great potential to remain stable over metal-aggregation and metal-dissolution, which are identified as the potentially highly active elements for ORR/OER. Especially, as the optimal bifunctional oxygen catalysts screened by this work, Co-Co/Ir-Qv3 display superior durability with a very negative E_{agg} value and a very positive U_{diss} value.

In addition, taking our identified high-active OER catalysts, namely Co-Co/Ir-NC, as an example, we experimental investigated the OER stability using chronoamperometry measurements at a constant current density of 10 mA cm^{-2}. As shown in **Supplementary Figs. 47 and 48**, the remarkable activities of Co-Co/Ir-NC can be well maintained at 10 mA cm^{-2} for 200 h with minimal degradation, demonstrating superior stability of our designed DACs compared to other reported carbon-based DACs, which is consistent with our computational results (**Supplementary Table 18**).

We have updated the statement in the manuscript *pages 14-15 and 17*:

The Pourbaix diagrams further reveals that the active sites of DACs are easily oxidized during OER, in line with previous reports[39], while the pristine dual-atom site is more favorable under the ORR condition (**Supplementary Figs. 26 and 27 and Supplementary Table 11**). OER prefer to occur along Path-II on *O-covered DACs rather than Path-I on pristine DACs (**Supplementary Figs. 28 and 29**). The similar volcano-like correlation between the descriptor ARSC and OER activities for DACs with the *O-covered active sites when k = 0.05 (**Supplementary Fig. 30**), suggesting the high universality of ARSC for OER. The smaller k also illustrates that OER is less sensitive to coordination effects compared to ORR, as the introduction of the same O-coordination will hinder the overall coordination effect governed by the difference of the N-coordination structures in the substrate. Some candidates with promising OER activity are identified, such as Co-Co-Qv3, Co-Ir-Qv3, and Co-Ni-Qv1 with U_L(OER) of 1.52 V, 1.52 V, and 1.53 V, respectively. These two volcano plots together show that the non-bonded DACs, especially Qv3-based DACs, can serve as promising bifunctional oxygen electrocatalysts, such as Co-Co/Ir-Qv3, due to their moderate value of ARSC.

39. Wygant, B. R., Kawashima, K. & Mullins, C. B. Catalyst or precatalyst? The effect of oxidation on transition metal carbide, pnictide, and chalcogenide oxygen evolution catalysts. *ACS Energy Lett.* **3**, 2956-2966 (2018).

As another crucial criterion for catalyst screening, we comprehensively evaluate the stability of the 840 DACs by calculating the aggregation energy (E_{agg}) and dissolution potential (U_{diss}). We use E_{agg} < 0 eV and U_{diss} > 0 V as the standard for the unaggregatable and indissoluble system[40]. **Supplementary Figs. 31-33** illustrate that the majority of X-Y-Qv2 and X-Y-Qv3 sites exhibit remarkable stability, while the metal atoms tend to aggregate and dissolve in the electrolyte in some X-Y-Qv4 and X-Y-Qv1 sites. It is worth noting that Fe, Co, Ni, Ru, Rh, Os, and Ir-based DACs have great potential to remain stable in a harsh electrochemical environment, which are identified as the potentially highly active elements for ORR/OER. Especially, as the optimal bifunctional oxygen catalysts screened by this work, Co-Co/Ir-Qv3 display superior durability with a very negative E_{agg} value and a very positive U_{diss} value.

Co-Co/Ir-NC can be well maintained at 10 mA cm^{-2} for 200 h with minimal degradation, demonstrating superior stability compared to other carbon-based DACs (**Supplementary Figs. 47 and 48 and Supplementary Table 18**).

We have provided the **Supplementary Tables 11 and 18** in the Supplementary Information:

Supplementary Table 11. Surface states of DACs under OER conditions via Pourbaix diagrams.

X-Y site	Qv4	Qv3	Qv2	Qv1
Co-Ni	*O	*O	*O	*O + *O
Co-Rh	*O + *OH	*O + *OH	*O + *OH	*O + *O
Co-Pd	*O	*O	*O	*O + *O

Co-Ir	*O + *O	*O + *O	*O + *O	*O + *O
Co-Pt	*O	*O	*O	*O + *O
Fe-Co	*O + *O	*O + *O	*O + *OH	*O + *O
Fe-Ni	*O + *O	*O + *OH	*O	*O + *O
Fe-Rh	*O + *O	*O + *O	*O + *O	*O + *O
Fe-Pd	*O	*O	*O	*O + *O
Fe-Ir	*O + *O	*O + *O	*O + *O	*O + *O
Fe-Pt	*O	*O	*O	*O + *O
Ru-Co	*O + *O	*O + *O	*O + *O	*O + *O
Ru-Ni	*O + *O	*O + *O	*O	*O + *O
Ru-Rh	*O + *O	*O + *O	*O	*O + *O
Ru-Pd	*O	*O	*O	*O + *O
Ru-Ir	*O + *O	*O + *O	*O + *O	*O + *O
Ru-Pt	*O	*O	*O	*O + *O
Os-Co	*O + *O	*O + *O	*O + *O	*O + *O
Os-Ni	*O + *O	*O + *O	*O + *O	*O + *O
Os-Rh	*O + *O	*O + *O	*O + *O	*O + *O
Os-Pd	*O	*O	*O	*O + *O
Os-Ir	*O + *O	*O + *O	*O + *O	*O + *O
Os-Pt	*O	*O	*O	*O + *O

Supplementary Fig. 18. OER stability comparison of Co-Co/Ir-NC with carbon-based DACs reported recently. The symbol '–' represents that the specific values have been not mentioned in the paper.

Electrocatalyst	Electrolytes	Durability time	η_{10} shift [activity loss]	Ref.
Co-Co-NC	1 M KOH	200 h	6 mV	This work
Co-Ir-NC	1 M KOH	200 h	8 mV	This work
FeN_4B-NiN_4B	0.1 M KOH	2000 cycles	10 mV	[31]
FeN_4-SC-NiN_4	0.1 M KOH	5000 cycles	9 mV	[32]
FeNi SAs/NC	0.1 M KOH	35 h	–	[3]
Fe-NiNC-50	1 M KOH	1500 cycles	2	[4]
$Ni_{66}Fe_{34}$-NC	0.1 M KOH	10000 s	[10.7%]	[5]
FeCo-NC	0.1 M KOH	5000 cycles	–	[7]
f-FeCo-CNT	0.1 M KOH	3000 cycles	10	[9]
FeNi-SAs@NC	1 M KOH	10 h/1000 cycles	–	[19]
IrCo−N−C	0.1 M KOH	2000 cycles	–	[21]
IrFe−N−C	1 M KOH	400 h	–	[24]
CoFe−N−C	1 M KOH	25 h	[3.4 %]	[26]
Fe/Ni(1:3)-NG	0.1 M KOH	1000 cycles	–	[27]

We have provided a description of the stability analysis in the *Method* section:

Stability analysis

The stability over metal-aggregation is governed by the aggregation energy (E_{agg}), which is defined as: $E_{agg} = (E(X\text{-}Y\text{-}NC) – E(NC) – \mu(X) – \mu(Y)) / 2$, where E(X-Y-NC) and E(NC) represent total energies of DACs and the defected nitrogenated graphene surface, respectively; μ(X) and μ(Y) are the energies of X-metal and Y-metal, which are taken from the bulk metals. The negative E_{agg} value indicates that the embedding

into graphene is preferred over metal clustering. Dissolution potential (U_{diss}) was used to determine the electrochemical stability against dissolution of X-Y sites[56], which is defined as: $U_{diss}(X) = U^{o}_{diss}(X) - (E(X\text{-}Y\text{-}NC) - E(Y\text{-}NC) - \mu(X)) / en_e$; $U_{diss}(Y) = U^{o}_{diss}(Y) - (E(X\text{-}Y\text{-}NC) - E(X\text{-}NC) - \mu(Y)) / en_e$; $U_{diss} = \min[U_{diss}(X), U_{diss}(Y)]$. In these equations, $U^{o}_{diss}(X)$ and $U^{o}_{diss}(Y)$ are the standard dissolution potential of bulk X-metal and Y-metal; n_e represent the number of transferred electrons involved in the dissolution; e is the electron charge; E(Y-NC) and E(X-NC) are the total energies of DACs with the vacancy of X-metal and Y-metal, respectively. The positive value of U_{diss} indicates that the dissolution of metal atoms can be better avoided under electrochemical reactions.

We have provided the statement in the *Method* section:

The OER stability was investigated using chronoamperometry measurements at a constant current density of 10 mA cm^{-2}.

We have provided the **Supplementary Figs. 26-33, 47, and 48** in the Supplementary Information:

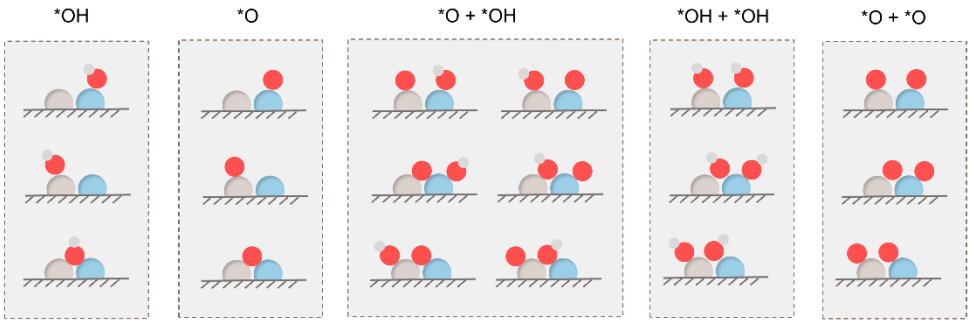

Supplementary Fig. 26. Adsorption of *O, *OH, *O + *OH, *OH + *OH, and *O + *O on DACs with all possible configurations. Blue, X-metal; grey, Y-mteal; red, O; white, H.

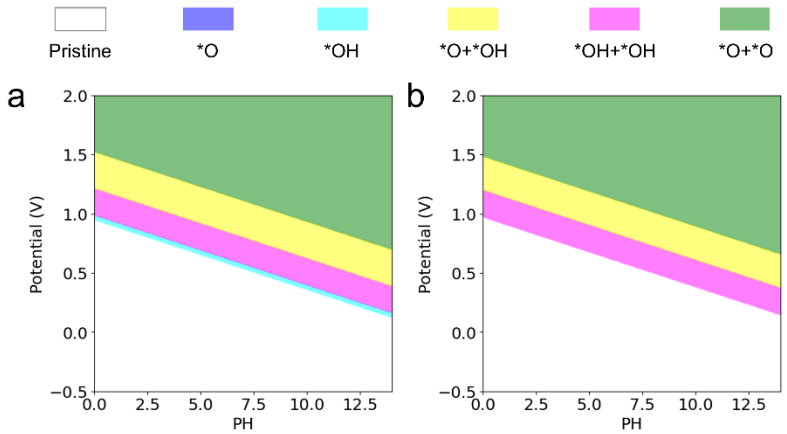

Supplementary Fig. 27. Pourbaix diagram of **a** Co-Co-Qv3 and **b** Co-Ir-Qv3. The Pourbaix diagrams are calculated using the Gibbs free energies of each intermediate on DACs at given U and pH.

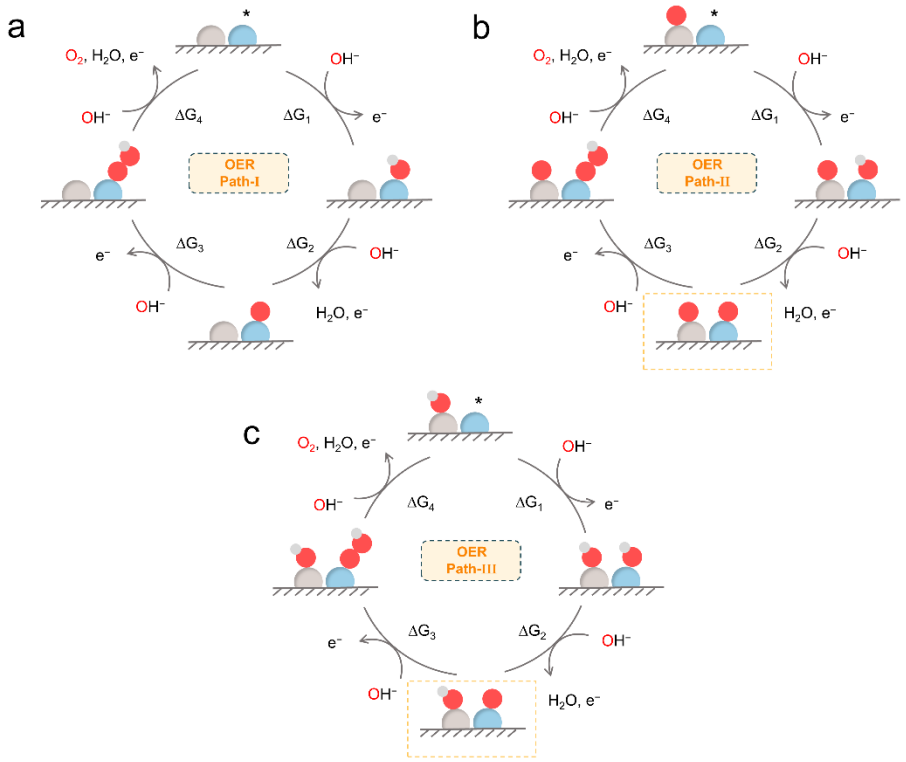

Supplementary Fig. 28. Schematic representation for the mechanisms of OER cycles on a X-Y dual-atom site. **a** Path-I, **b** Path-II (surface states of *O + *O), and **c** Path-III (surface states of *O + *OH). Blue, X-metal; grey, Y-mteal; red, O; white, H.

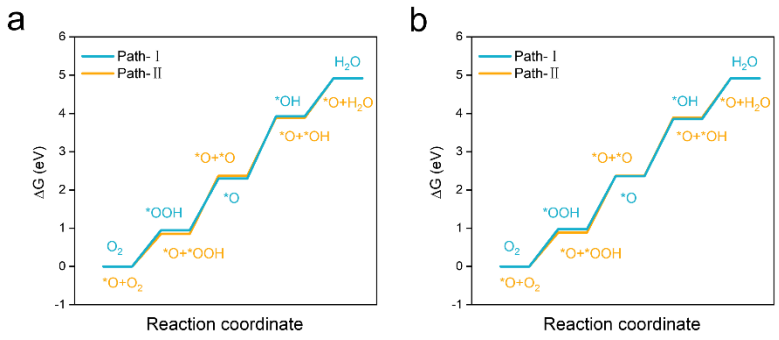

Supplementary Fig. 29. Calculated free energy profiles of Path-I and Path-II for ORR on **a** Co-Co-Qv3 and **b** Co-Ir-Qv3.

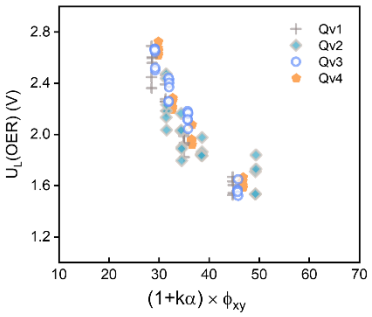

Supplementary Fig. 30. Volcano relationship between U_L(OER) versus ARSC, defined as $(1 + k\alpha) \times \phi_{xy}$ on X-Y sites. X is Ru, Os, Fe, and Co; Y is Co, Ni, Rh, Pd, Ir, and Pt.

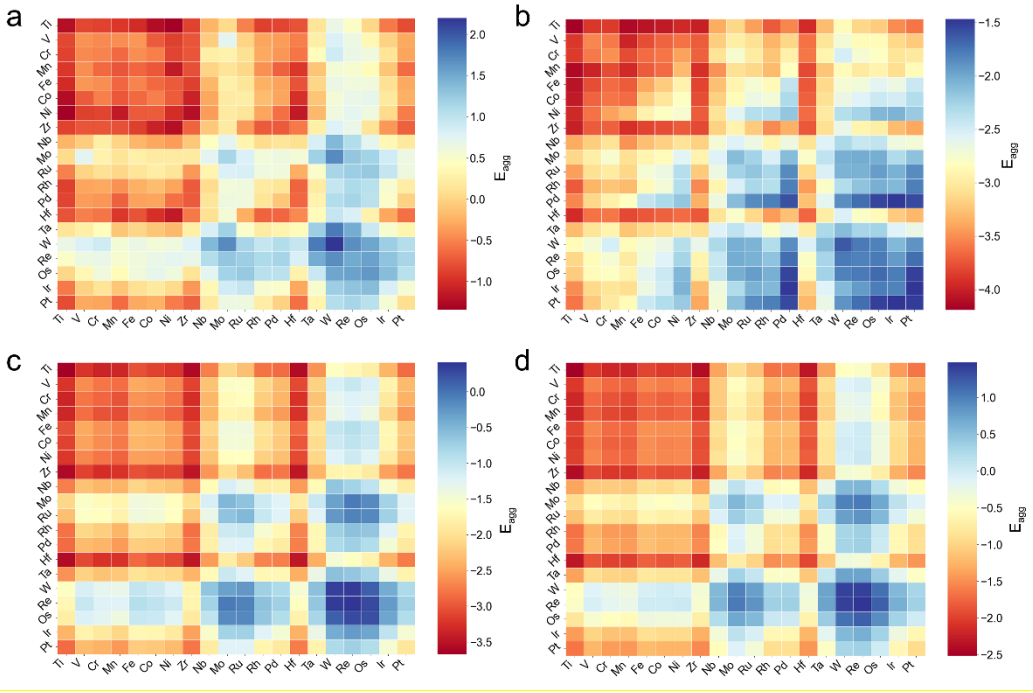

Supplementary Fig. 31. Heatmap of aggregation energy (E_{agg}) for 840 DACs, including **a** X-Y-Qv1, **b** X-Y-Qv2, **c** X-Y-Qv3, and **d** X-Y-Qv4.

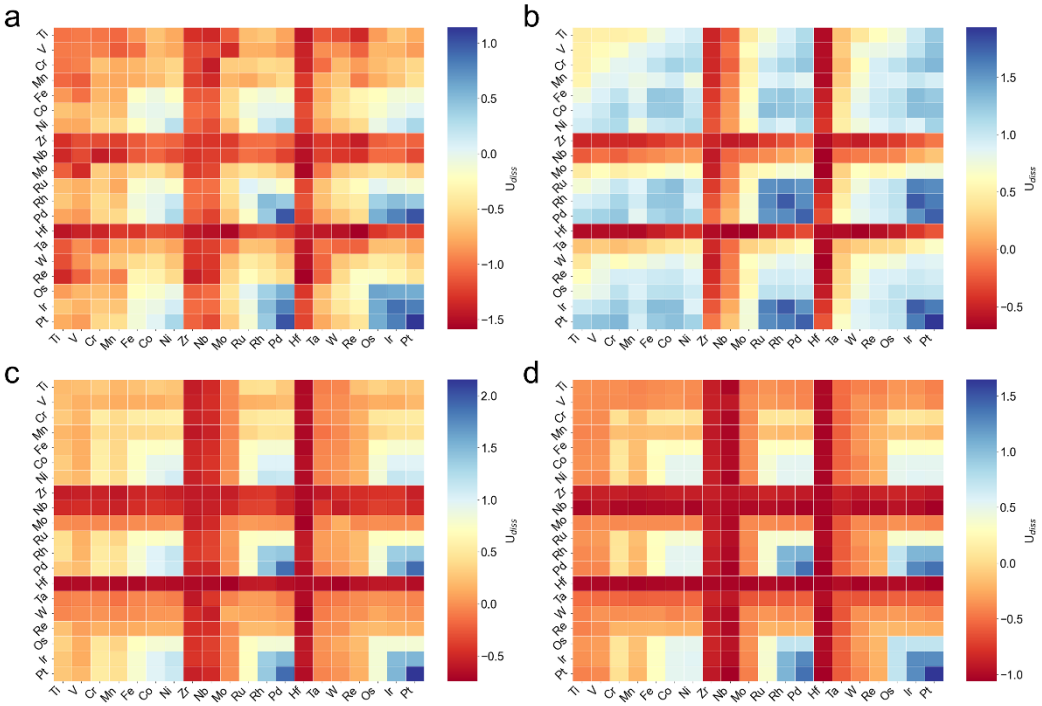

Supplementary Fig. 32. Heatmap of dissolution potential (U_{diss}) for 840 DACs, including **a** X-Y-Qv1, **b** X-Y-Qv2, **c** X-Y-Qv3, and **d** X-Y-Qv4.

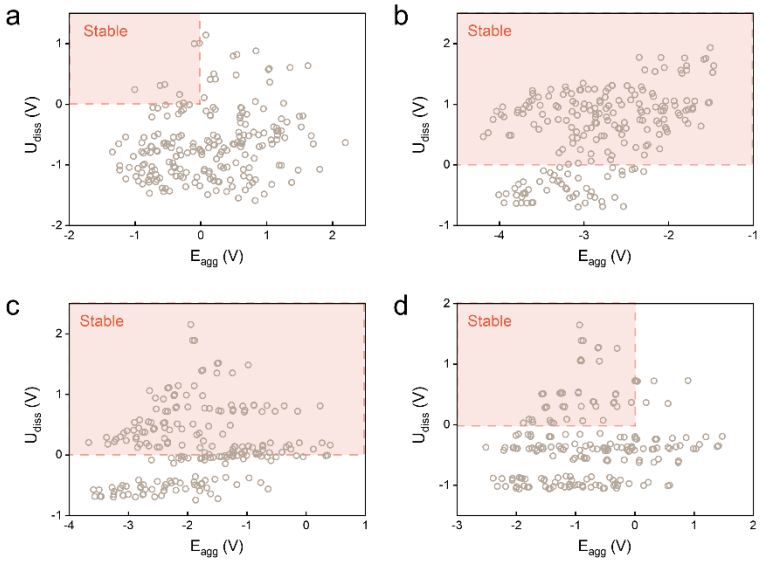

Supplementary Fig. 33. Computed aggregation energy (E_{agg}) and dissolution potential (U_{diss}) for 840 DACs, including **a** X-Y-Qv1, **b** X-Y-Qv2, **c** X-Y-Qv3, and **d** X-Y-Qv4.

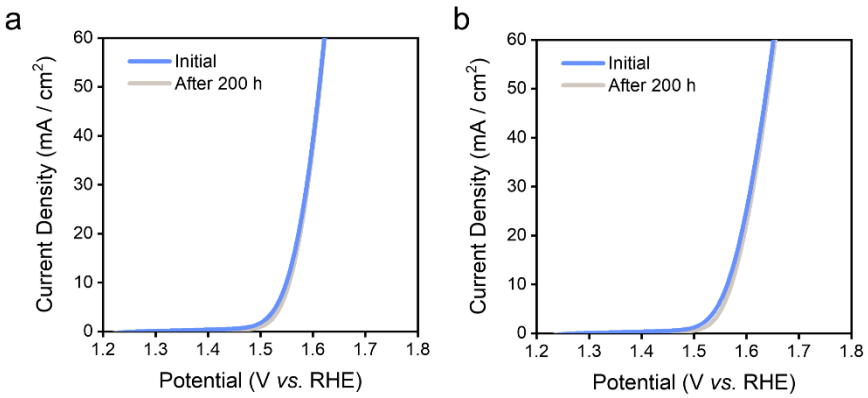

Supplementary Fig. 47. OER polarization curves of **a** Co-Co-NC and **b** Co-Ir-NC before and after 200-h-long working at 10 mA cm^{-2}.

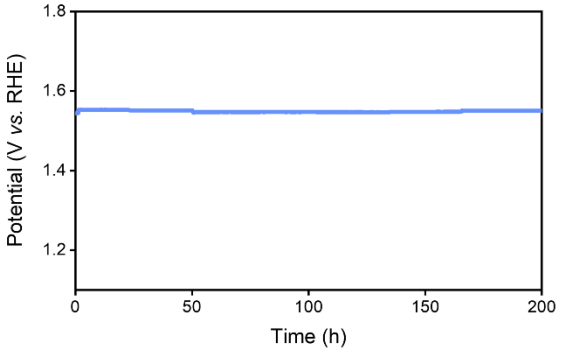

Supplementary Fig. 48. Chronopotentiometric curves of Co-Co-NC at a constant current density of 10 mA cm^{-2}.

Reviewer #2:

General Comments R2: *Dual-atom catalysts, possessing the synergistic effects between the two atoms, have increasingly garnered attention due to their unique, tunable chemical and physical properties, as well as their catalytic performance. One significant challenge in designing DAC through a bottom-up approach lies in the immense variety of atomic parings, support choices, and coordination environment changes. This complexity greatly limits the feasibility of direct density functional theory (DFT) calculations which requires substantial computational resources.*

In this work, Lin et al. introduce an Interpretable machine learning approach (ARSC) to conduct high-throughput catalyst screening, incorporating the atomic property (A), reactant (R), synergistic (S), and coordination effects (C). Starting from the physical foundation of the d-band theory, they propose a primitive descriptor considering the d-band filling (f_d) and width (W_d) from three electrocatalysis reactions (ORR/OER, CRR, and NRR) over homonuclear DACs, followed by the transformation to the physical properties of the elements that closely related to the fd and wd. Moving forward, the descriptor is refined i) based on the reaction types through the feature engineering approach and ii) by considering the coordination effects. In the end, the well-developed descriptor is applied for catalyst screening and the prediction is validated through experimental effort.

Overall, by leveraging the DFT calculations and ML approach, this work introduces a simple well-refined descriptor, achieves the high throughout catalyst screening, and conducts the experimental validation. It is an interesting, timely, and well-ordered work regarding the rising attention towards the DACs in catalysis and the application of Machine learning in catalyst screen and design. However, to the best of my knowledge, there are several comments that should be addressed to deepen the understanding and enhance the overall quality of this work prior to publication.

Response: Many appreciations to the reviewer for the positive evaluation and constructive suggestions on our work. Your valuable comments have greatly improved the overall quality and research depth of our work. We have seriously considered your comments, supplemented the related calculations and discussions, and improved our manuscript based on your points.

Specific Comment R2-1: *The physical basis of this work is the d-band theory which is typically applied to the heterogeneous system such as metal surfaces and nanoparticles. However, SAC and DAC resemble homogeneous systems and demonstrates the molecular complex characteristics, it is questionable to apply the d-orbital theory for DACs. Recent works on SAC demonstrates that the frontier orbitals play the essential role in determining the interactions between species and the catalyst, as evidenced by publications in PRL, 2020, 125, 156001, ACS Catal. 2024, 14, 2, 886–896, and Angew. Chem. Int. Ed. 2024, 63, e202311174. Given that i) some of the d-orbitals participate in forming bonds with the supports and ii) the frontier orbitals mostly contribute to the adsorbate bindings. Shifting the d-band theory*

(which containing all d-orbitals) to the specific frontier d-orbitals (main contributor to the adsorptions) could offer deeper physical insight and aid in developing more accurate descriptors for DACs.

Response: We thank the reviewer for the useful comment very much. We fully agree that since dual-atom sites incorporate some characteristics of homogeneous systems, further investigation into the influence of frontier orbitals can help us better understand the structure-performance relationship of DACs. According to the reviewer's valuable suggestion, we re-plotted projected density of states (PDOS) of all X-X sites. **Supplementary Fig. 8** shows that the d-orbitals of DACs are distinct compared with that of metal atoms or metal surfaces, lying between energy levels and energy bands. The d-orbitals of the early transition metals exhibit properties closer to energy bands, such as Ti, Zr, Hf, and Ta, where d-orbitals become broad and continuous, accompanied by the overlapping of d_{xy}, d_{xz}, $d_{x^2-y^2}$, d_{yz}, and d_{z^2}. In contrast, as the number of d electrons increases, the splitting of the d-orbitals into discrete levels becomes stronger, and the difference between different orbitals becomes more pronounced, especially for Ni, Pd, and Pt whose d-orbital characteristics are similar with the literature reports (**R. Wu** et al., *Phys. Rev. Lett.* 2020, 125, 156001; **D. G. Vlachos** et al., *ACS Catal.* 2024, 14, 2, 886–896; **S. Caratzoulas** et al., *Angew. Chem. Int. Ed.* 2024, 63, e202311174). It seems that using either the d-orbital theory or the frontier orbital theory alone cannot adequately describe these specific d-orbital properties of DACs. Therefore, we combined the d-band theory and the frontier orbitals to comprehensively quantify the impact of the distinct, non-continuous d-orbital properties of dual-atom sites on adsorption ability.

First, we determined the frontier d-orbitals of DACs and studied their correlation with adsorption ability, taking ΔG(*OH) as an example. **Supplementary Fig. 10a** show that the energy level of the frontier orbital of DACs scales linearly with ΔG(*OH), suggesting that the frontier orbitals (FO) mainly contribute to the binding with adsorbates, which is consistent with the previous work (**D. G. Vlachos** et al., *ACS Catal.* 2024, 14, 2, 886–896). It can be explained that due to the electron transfer from the metal to *OH, the farther the highest occupied molecular orbital (HOMO) of the metal center is from the Fermi level (E_f), the less favorable it is for accepting electrons of *OH, leading to a decrease in the metal-OH interaction. d_{xz}, d_{yz}, and d_{z^2} is found to be FO for most metals, while $d_{x^2-y^2}$ and d_{xy} locate further away from E_f. The importance of FO is further verified by the integrated crystal orbital Hamilton population (ICOHP) analysis, which indicates that the metal-OH interaction mainly stems from d_{xz}, d_{yz}, and d_{z^2}, whereas $d_{x^2-y^2}$ and d_{xy} contribute little (**Supplementary Fig. 10b**). This phenomenon is influenced by the adsorption configuration. Only the d-orbital vertical to the catalyst surface can effectually overlap with s/p orbitals of the adsorbed O, therefore d_{xz}, d_{yz}, and d_{z^2} play a primary role in bonding with *OH (**J. Gong** et al., *Angew. Chem. Int. Ed.* 2023, 62, e202300122; **Z. Xia** et al., *Adv. Energy*

Mater. 2019, 9, 1902625). However, although we have confirmed that FO dominate the metal's adsorption capacity, due to the characteristics of the energy bands remaining in DACs, if we do not consider the shape of FO (d_{xz}, d_{yz}, and d_{z^2}), using only the position of the energy levels cannot be precisely correlated with the adsorption energies (R^2 = 0.87, **Supplementary Fig. 10a**).

We incorporated the d-band theory to further improve the accuracy of adsorption energy description based on FO. In our previous submission, we found that the relative antibonding position of the whole d-orbital (f_d / $W_d^{0.5}$) can serve as an electronic descriptor for understanding the effect of the d-band shape on adsorption properties on dual-atom sites. Based on our exploration of the frontier orbitals, we more deeply concluded that the different adsorption capacities of metals originate from the relative antibonding positions of FO (f_{FO} / $W_{FO}^{0.5}$), which can be verified by the linear relationship between f_{FO} / $W_{FO}^{0.5}$ and ΔG(*OH) with R^2 = 0.94 (**Supplementary Fig. 10c**). However, given that atomic properties of metals may fail to describe the properties of some specific orbitals in the whole d-orbitals when coordinating with N atoms, using only properties of frontier orbitals would make it difficult to construct a low-cost intrinsic descriptor. A better approach is to relate the properties of FO to those of the whole d-orbitals, and then correlate them with atomic properties. **Supplementary Fig. 10d** shows a strongly linear relationship between f_{FO} / $W_{FO}^{0.5}$ and f_d / $W_d^{0.5}$ with R^2 = 0.98, indicating that the d-band shape can well describe the structure-activity relationship of DACs, and the primitive descriptor ϕ_{xx} constructed via f_d / $W_d^{0.5}$ can also quantify the impact of the shape of FO on the adsorption energies.

In conclusion, **since the distinct d-orbitals of DACs lie between energy levels and energy bands, we combined the d-band theory and the frontier orbitals to develop descriptors, that is, we found that the shape of FO (d_{xz}, d_{yz}, and d_{z^2}) and all d-orbitals both can clarify the structure-activity relationship with comparable accuracy.**

We have provided the statement in the *Introduction* section:

Moreover, distinguished from metallic catalysts, many previous works have reported that the frontier orbitals (FO) play an essential role in determining adsorption capacity for SACs due to their molecular complex characteristics in d-orbitals[33-35]. As a result, accurately quantifying the impact of its distinct d-orbital on activity is of utmost importance for DACs design.

33. Fu, Z., Yang, B. & Wu, R. Understanding the activity of single-atom catalysis from frontier orbitals. *Phys. Rev. Lett.* **125**, 156001 (2020).

34. Li, Q., Yan, G. & Vlachos, D. G. Theoretical insights into H_2 activation over anatase TiO_2 supported metal adatoms. *ACS Catal.* **14**, 886-896 (2024).

35. Yang, P., Li, J., Vlachos, D. G. & Caratzoulas, S. Tuning active site flexibility by defect engineering of graphene ribbon edge-hosted Fe-N_3 sites. *Angew. Chem. Int. Ed.* **63**, e202311174 (2024).

The physical meaning of PFESS is based on our combination of d-band theory and the frontier orbitals.

We have updated the statement in the manuscript *pages 5-6*:

However, given that d-orbitals of DACs lie between energy levels and energy bands (**Supplementary Figs. 4-8**), relying solely on the d-band center no longer effectively describes adsorption capability (**Supplementary Fig. 9**). Alternatively, we find that d_{xz}, d_{yz}, and d_{z^2} are found to be FO for most DACs, and using the energy levels of FO will further enhance the accuracy of describing adsorption energies (**Supplementary Fig. 10a,b**). However, the lack of consideration for the d-band shape results in insufficient precision, due to the characteristics of the energy bands remaining in DACs.

Our calculations further reveal that the shape of FO (f_{FO} / $W_{FO}^{0.5}$) is strongly correlated with the d-band shape, indicating that the FO and all d-orbitals both can effectively describe the structure-activity relationship of DACs with comparable accuracy (**Supplementary Fig. 10c,d**).

We have provided the **Supplementary Figs. 8 and 10** in the Supplementary Information:

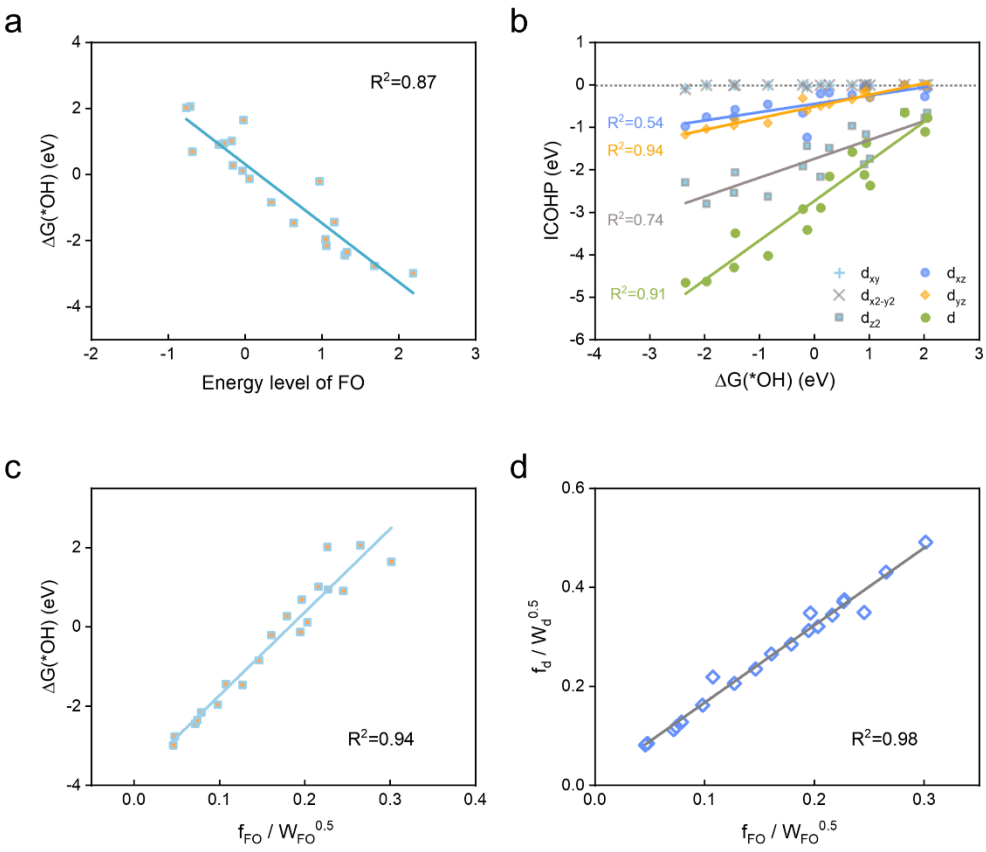

Supplementary Fig. 10. a ΔG(*OH) as a function of the energy level of frontier orbitals (FO) on X-X-Qv3. **b** Linear relationship between integrated crystal orbital Hamilton population (ICOHP) for bond between d-orbitals of metals and adsorbates

versus ΔG(*OH) on X-X-Qv3. **c** ΔG(*OH) as a function of $f_{FO} / W_{FO}^{0.5}$ in X-X-Qv3. **d** $f_d / W_d^{0.5}$ as a function of $f_{FO} / W_{FO}^{0.5}$ in X-X-Qv3.

Specific Comment R2-2: *Beyond the extensive combinations of X-Y that limits the DFT efforts for searching the optima catalysts, the stability of DACs presents as another crucial criterion for catalyst screening. In the context of the 840 DACs, assessing their stability becomes imperative. How should their stability be evaluated? If the catalyst is highly unstable, what is the meaning to conduct DFT calculations?*

Response: We are very grateful to the reviewers for your helpful comments, which we really did not consider in previous submission. Inspired by your kind reminder, we have comprehensively evaluated the stability of the 840 DACs, including the thermodynamic and electrochemical stability. This method is widely used in the stability assessment of metal-doped graphene-based systems, and its reliability and feasibility have been confirmed by many experimental and computational studies (**X. Sun** et al., *Nat. Commun.* 2023, 14, 4449; **K. S. Kim** et al., *Energy Environ. Sci.* 2021, 14, 3455–3468).

The stability over metal-aggregation is governed by the aggregation energy (E_{agg}), which is defined as:

$$E_{agg} = (E(X\text{-}Y\text{-}NC) - E(NC) - \mu(X) - \mu(Y)) / 2$$

where E(X-Y-NC) and E(NC) represent total energies of DACs and the defected nitrogenated graphene surface, respectively; μ(X) and μ(Y) are the energies of X-metal and Y-metal, which are taken from the bulk metals. The negative E_{agg} value indicates that the embedding into graphene is preferred over metal clustering. The E_{agg} values for all 840 DACs are summarized in **Supplementary Fig. 31**. The results show that X-Y-Qv2 and X-Y-Qv3 are slightly more stable against clustering than X-Y-Qv4 and notably more stable than X-Y-Qv1. The majority of X-Y-Qv2 and X-Y-Qv3 sites exhibit sufficiently negative E_{agg}, suggesting the strong interaction between the dispersed X-Y sites and the coordination N atoms.

Furthermore, we utilized dissolution potential (U_{diss}) to determine the electrochemical stability against dissolution of X-Y sites (**J. K. Nørskov** et al., *Electrochim. Acta* 2007, 52, 5829–5836), which is defined as:

$$U_{diss}(X) = U^{o}_{diss}(X) - (E(X\text{-}Y\text{-}NC) - E(Y\text{-}NC) - \mu(X)) / en_e$$

$$U_{diss}(Y) = U^{o}_{diss}(Y) - (E(X\text{-}Y\text{-}NC) - E(X\text{-}NC) - \mu(Y)) / en_e$$

$$U_{diss} = \min[U_{diss}(X), U_{diss}(Y)]$$

where $U^{o}_{diss}(X)$ and $U^{o}_{diss}(Y)$ are the standard dissolution potential of bulk X-metal and Y-metal; n_e represent the number of transferred electrons involved in the dissolution; e is the electron charge; E(Y-NC) and E(X-NC) are the total energies of DACs with the vacancy of X-metal and Y-metal, respectively. The positive value of U_{diss} indicates that the dissolution of metal atoms can be better avoided under electrochemical

reactions. As shown in **Supplementary Fig. 32**, X-Y-Qv2 and X-Y-Qv3 sites is more likely to maintain durability in a harsh electrochemical environment.

The stability of 840 DACs was comprehensively evaluated by plotting E_{agg} versus U_{diss} (**Supplementary Fig. 33**). We used E_{agg} < 0 eV and U_{diss} > 0 V as the standard for the unaggregatable and indissoluble system. The more negative the E_{agg} value and the more positive the U_{diss} value, the stronger the stability of DACs. It is found that the majority of X-Y-Qv2 and X-Y-Qv3 sites exhibit remarkable stability, while the metal atoms tend to aggregate and dissolve in the electrolyte in some X-Y-Qv4 and X-Y-Qv1 sites. For CRR and NRR, our study has suggested that the CRR and NRR activities are not sensitive to the coordination effects. Therefore, according to the screened X-Y combinations, synthesizing DACs with the Qv2 and Qv3 coordination structure is more likely to gain better catalytic performance. For OER and ORR, our calculations show that Fe, Co, Ni, Ru, Rh, Os, Ir-based DACs have great potential to remain stable over metal-aggregation and metal-dissolution, which are identified as the potentially highly active elements for ORR/OER. Especially, as the optimal bifunctional oxygen catalysts screened by this work, Co-Co/Ir-Qv3 display superior durability with a very negative E_{agg} value and a very positive U_{diss} value.

In conclusion, since most DACs have great potential to be stable in a harsh electrochemical environment, especially for our identified high-efficiency X-Y sites, our investigation of the selectivity and activity of DACs for multiple reactions is of great significance in this work.

We have provided the statement in the manuscript *page 14*:

As another crucial criterion for catalyst screening, we comprehensively evaluate the stability of the 840 DACs by calculating the aggregation energy (E_{agg}) and dissolution potential (U_{diss}). We use E_{agg} < 0 eV and U_{diss} > 0 V as the standard for the unaggregatable and indissoluble system[40]. **Supplementary Figs. 31-33** illustrate that the majority of X-Y-Qv2 and X-Y-Qv3 sites exhibit remarkable stability, while the metal atoms tend to aggregate and dissolve in the electrolyte in some X-Y-Qv4 and X-Y-Qv1 sites. It is worth noting that Fe, Co, Ni, Ru, Rh, Os, and Ir-based DACs have great potential to remain stable in a harsh electrochemical environment, which are identified as the potentially highly active elements for ORR/OER. Especially, as the optimal bifunctional oxygen catalysts screened by this work, Co-Co/Ir-Qv3 display superior durability with a very negative E_{agg} value and a very positive U_{diss} value.

We have provided the **Supplementary Figs. 31-33** in the Supplementary Information:

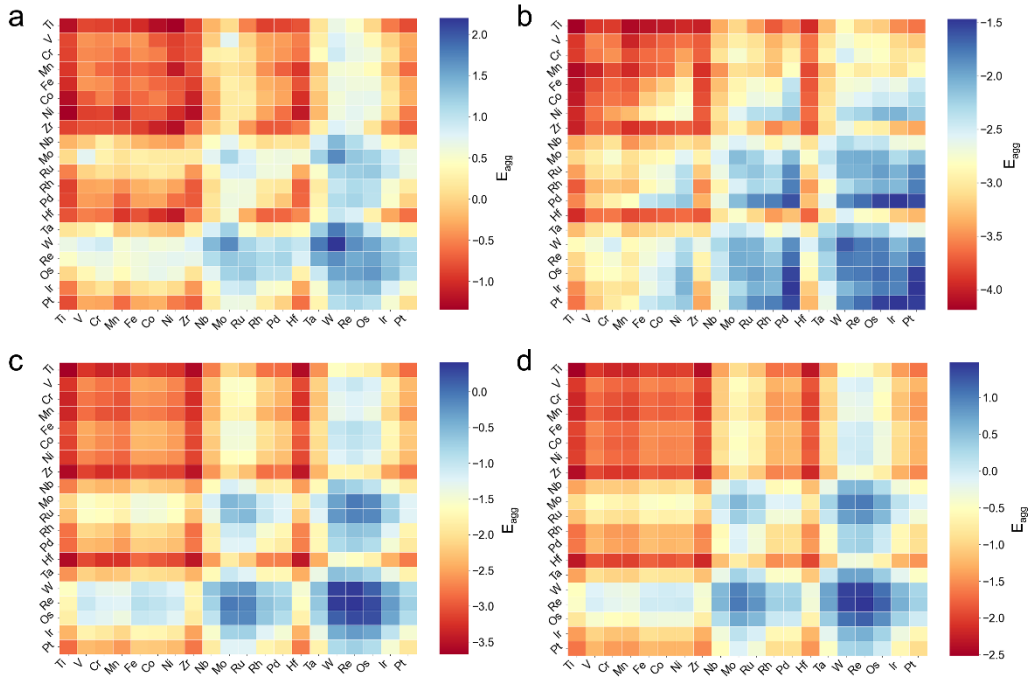

Supplementary Fig. 31. Heatmap of aggregation energy (E_{agg}) for 840 DACs, including **a** X-Y-Qv1, **b** X-Y-Qv2, **c** X-Y-Qv3, and **d** X-Y-Qv4.

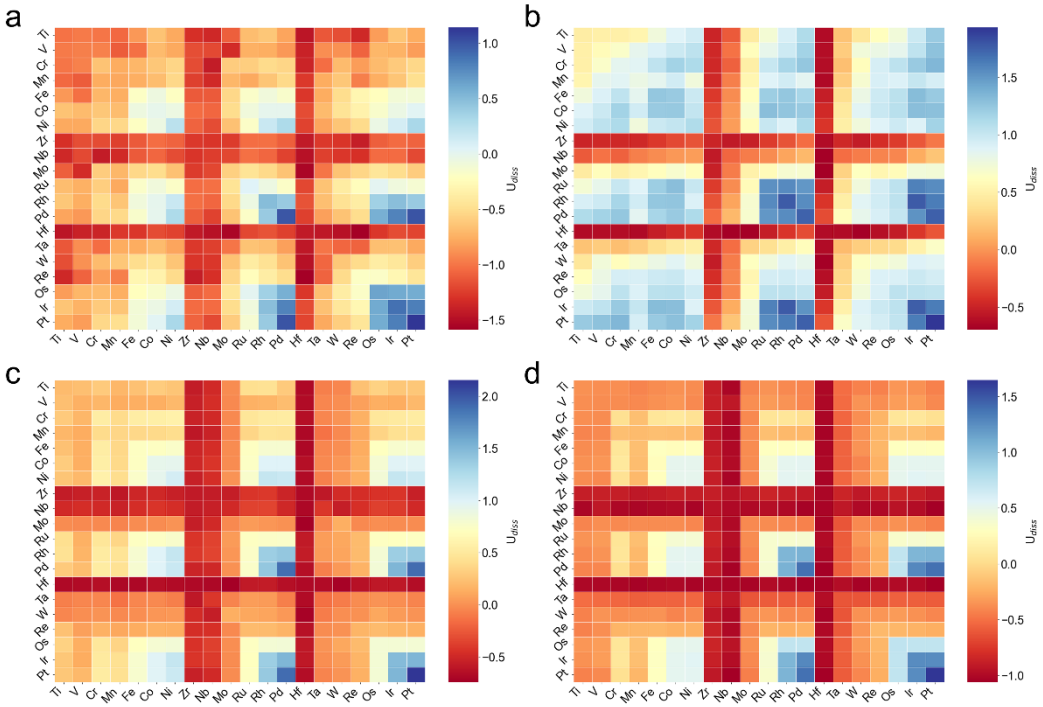

Supplementary Fig. 32. Heatmap of dissolution potential (U_{diss}) for 840 DACs, including **a** X-Y-Qv1, **b** X-Y-Qv2, **c** X-Y-Qv3, and **d** X-Y-Qv4.

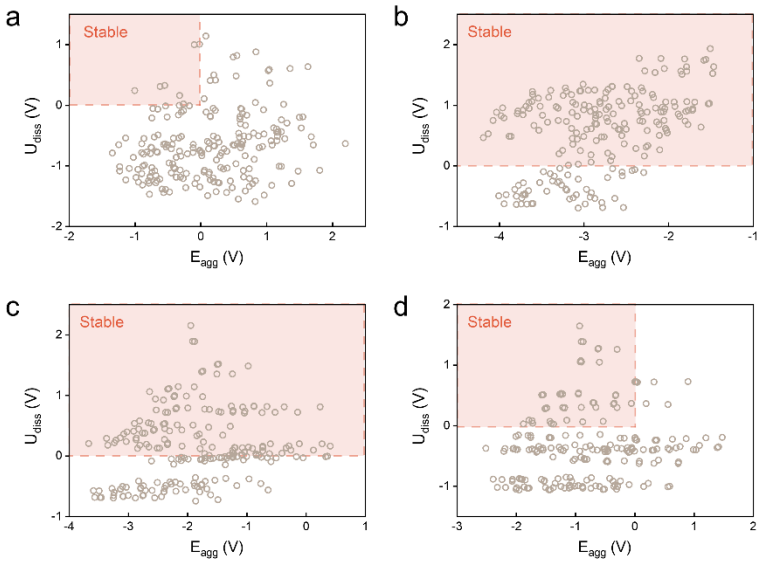

Supplementary Fig. 33. Computed aggregation energy (E_{agg}) and dissolution potential (U_{diss}) for 840 DACs, including **a** X-Y-Qv1, **b** X-Y-Qv2, **c** X-Y-Qv3, and **d** X-Y-Qv4.

We have provided a description of the stability analysis in the *Method* section:

Stability analysis

The stability over metal-aggregation is governed by the aggregation energy (E_{agg}), which is defined as: $E_{agg} = (E(X\text{-}Y\text{-}NC) - E(NC) - \mu(X) - \mu(Y)) / 2$, where E(X-Y-NC) and E(NC) represent total energies of DACs and the defected nitrogenated graphene surface, respectively; μ(X) and μ(Y) are the energies of X-metal and Y-metal, which are taken from the bulk metals. The negative E_{agg} value indicates that the embedding into graphene is preferred over metal clustering. Dissolution potential (U_{diss}) was used to determine the electrochemical stability against dissolution of X-Y sites[56], which is defined as: $U_{diss}(X) = U^{o}_{diss}(X) - (E(X\text{-}Y\text{-}NC) - E(Y\text{-}NC) - \mu(X)) / en_e$; $U_{diss}(Y) = U^{o}_{diss}(Y) - (E(X\text{-}Y\text{-}NC) - E(X\text{-}NC) - \mu(Y)) / en_e$; $U_{diss} = \min[U_{diss}(X), U_{diss}(Y)]$. In these equations, $U^{o}_{diss}(X)$ and $U^{o}_{diss}(Y)$ are the standard dissolution potential of bulk X-metal and Y-metal; n_e represent the number of transferred electrons involved in the dissolution; e is the electron charge; E(Y-NC) and E(X-NC) are the total energies of DACs with the vacancy of X-metal and Y-metal, respectively. The positive value of U_{diss} indicates that the dissolution of metal atoms can be better avoided under electrochemical reactions.

Specific Comment R2-3: *In Section , the author mentioned that "Wd is solely influenced by the d-orbital size, presenting as a negative function of atomic radius (R) and the number of electron shells (S) (Wd $\propto$ 1/(R×S))". However, the description of the atomic radius is ambiguous. There are several types of atomic radius using in chemistry. It can be inferred from the values that "R" is the atomic radii computed from theoretical models by Enrico Clement (J. Chem. Phys. 47, 1300–1307 (1967). As metal atom binds to N and possesses positive charges, why not using Ionic radius? In addition, what are the behaviors of metallic radius and covalent radius?*

Response: We thank the reviewer for this kind suggestion. We fully agree that, besides the atomic radii we currently use, it is necessary to clarify whether other types of atomic radii can also accurately quantify the structure-performance relationship of dual-atom sites. The atomic radii we used in this work are calculated using self-consistent-field (SCF) functions (**W. P. Reinhardt** et al., *J. Chem. Phys.* 1963, 38, 2686−2689; **W. P. Reinhardt** et al., *J. Chem. Phys.* 1967, 47, 1300–1307). This type of atomic radii has been widely used to develop intrinsic descriptors of active sites to deeply clarify the structure-activity relationship on metal-doped NC-based systems (**Z. Xia** et al., *Adv. Energy Mater.* 2019, 9, 1902625; **X. Zhang** et al., *J. Mater. Chem. A* 2022, 10, 18803). After carefully considering the reviewer's comments, we further compared the ionic radius, covalent radius, and metallic radius to determine which one is more suitable for describing the atomic property effect of DACs. We performed electron localization function (ELF) to reveal the bonding types between the metal center and the coordination N atoms. An ELF value close to 1 (> 0.5) between two atoms represents a covalent bond; a value < 0.5 at one atom and a value close to 1 at the other atom represents an ionic bond; a value = 0.5 represents the electron-gas-like pair, that is, metallic bond (**K. E. Edgecombe** et al., *J. Chem. Phys.*, 1990, 92, 5397–5403). Taking Co-Co-Qv3 as an example, **Supplementary Fig. 55** shows a high ELF value close to 1 between Co atom and coordination N atom, indicating strong covalent bond characteristics. The integrated crystal orbital Hamilton population (ICOHP) value for Co-N bonds is around –4 eV, further suggesting the stable covalent bonds. The metal-N covalent bonding can also be widely observed for other DACs. All these results demonstrate that although metal atom binds to N and possesses positive charges, metals tend to form stable covalent bonds with the coordination N atoms, which is consistent with the previously reported research (**C. L. Wu** et al., *J. Mater. Chem. A,* 2022, 10, 9048–9058). Therefore, it seems that covalent radius is more suitable for quantifying atomic property effects of metal center on the catalytic performance. As shown in **Supplementary Fig. 56a,b**, similar to the atomic radii based on SCF functions, ϕ_{xx} calculated by covalent radii (derived from *CRC Handbook of Chemistry and Physics*) also present linear relationships with $\Delta G(*COOH)$, $\Delta G(*OH)$, and $\Delta G(*N_2 \rightarrow *N_2H)$. The predictive accuracy of these two types of radii is comparable, slightly superior to metallic radii (**Supplementary Fig. 56c**, derived from **A.F. Wells**, *Structural Inorganic Chemistry 5th ed., Clarendon Press,* Oxford, 1984, 1288). Another advantage of the covalent radii over the ionic radii is that the covalent radii can be directly obtained from databases at zero cost, whereas the ionic radii depend on the oxidation state of metal ions, which requires complicated confirmation through DFT calculations and experimental characterization. Therefore, using the ionic radii as atomic properties goes against our original intention of reducing costs and improving efficiency of high-throughput screening of DACs. Some experiments have also confirmed that metal atoms coordinated with nitrogen may exhibit mixed valence states (**H. L. Xin** et al., *Angew. Chem. Int. Ed.* 2019, 58, 2321–2325), which further suggests that a certain value of ionic radii is impossible to represent the chemical state of a metal center. In conclusion, considering the real bonding state of the metal center in DACs, as well as the cost and

availability of our developed descriptors, **we have demonstrated that covalent radii are superior to the metallic and ionic radii, which can also be used to describe the atomic property effect in DAC system with a high accuracy like that of the atomic radii based on SCF functions.**

We have provided a description in the *Method* section:

Atomic properties selection

The atomic radii *R* we used in this work are calculated using self-consistent-field (SCF) functions[55]. We also considered and compared the ionic radii, covalent radii, and metallic radii as *R* values. The results of electron localization function (ELF) reveal strong covalent bond characteristics between metal centers and coordination N atoms on DACs (**Supplementary Fig. 55**), suggesting that covalent radii are more suitable for quantifying atomic property effects of metal center on the catalytic performance than ionic radii and metallic radii. The descriptor based on covalent radii (derived from *CRC Handbook of Chemistry and Physics*) demonstrates a predictive accuracy comparable to that based on the SCF function-calculated atomic radii (**Supplementary Fig. 56**), indicating that the covalent radii can also be used as *R* in this work. While the ionic radii and metallic radii may be not suitable, which suffers from high costs and low accuracy, respectively.

We have provided the **Supplementary Figs. 55 and 56** in the Supplementary Information:

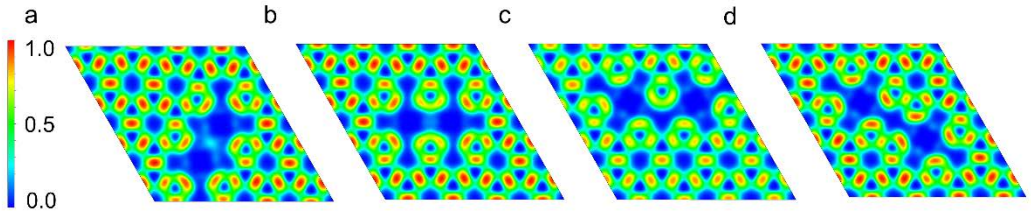

Supplementary Fig. 55. The electron localization function (ELF) of **a** Co-Co-Qv1, **b** Co-Co-Qv2, **c** Co-Co-Qv3, and **d** Co-Co-Qv4.

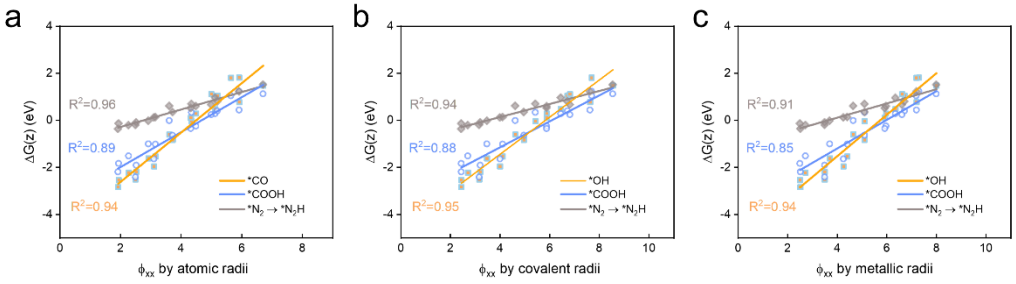

Supplementary Fig. 56. ΔG(*COOH), ΔG(*OH), or ΔG(*N_2 → *N_2H) as functions of ϕ_{xx} based on **a** atomic radii, **b** covalent radii, and **c** metallic radii on X-X sites.

Specific Comment R2-4: *In figure 2e and other figures related to linear scaling relations (LSRs), the broad energy span and large dataset facilitate achieving an ideal R2 value effortlessly. It is recommended that the authors to thoroughly evaluate the LSRs by including more regression results such as mean absolute error, maximum positive/negative error and root mean square errors.*

Response: We thank the reviewer for this important suggestion. We have supplemented the comprehensive assessment of LSRs mentioned in this manuscript, including **Figs. 2b-e, Fig. 2g, Figs. 4c-e, and Supplementary Fig. 14**, as listed in **Supplementary Table 23**. Our results show no extremely obvious outliers in LSRs. The root mean square errors (RMSE) is more sensitive to outliers compared to the mean absolute error (MAE), and RMSE is particularly useful when larger errors should be penalized more. As well as R^2, RMSE has been widely used as an important metric to evaluate the goodness of LSRs. The largest RMSE for LSR between ϕ_{xx} and adsorption energies of various key intermediates is below 0.4 eV, comparable and even lower than that reported in the literature (**T. P. Senftle** et al., *Nat. Catal.* 2018, 1, 531–539), demonstrating the superior prediction performance of our simple descriptor ϕ_{xx}. More importantly, after incorporating the synergistic effect and using our developed PFESS algorithm, the RMSE for ϕ_{xy} is decreased to below 0.1 eV, exhibiting a more remarkable prediction accuracy.

We have provided a description in the *Method* section:

Evaluation of linear scaling relations.

In addition to the R^2 mentioned in the figure, we listed multiple regression results for the linear scaling relations (LSRs) in **Figs. 2b-e, Fig. 2g, Figs. 4a-c, and Supplementary Fig. 14**, including the mean absolute error (MAE), maximum positive/negative error (MPE/MNE) and root mean square errors (RMSE), as shown in **Supplementary Table 23**.

We have provided the **Supplementary Table 23** in the Supplementary Information:

Supplementary Table 23. The mean absolute error (MAE), maximum positive/negative error (MPE/MNE) and root mean square errors (RMSE) for linear scaling relations.

Fig.	y-x	R^2	MAE	MPE	MNE	RMSE
2e	$\Delta G(*OH)$-ϕ_{xx}	0.937	0.309 eV	0.845 eV	–0.596 eV	0.385 eV
2e	$\Delta G(*COOH)$-ϕ_{xx}	0.90	0.291 eV	0.803 eV	–0.773 eV	0.371 eV
14	$\Delta G(*N_2 \rightarrow *N_2H)$-$\phi_{xx}$	0.959	0.080 eV	0.172 eV	–0.288 eV	0.105 eV
2b	$\Delta G(*OH)$-f_d / $W_d^{0.5}$	0.932	0.330 eV	0.888 eV	–0.596 eV	0.400 eV
2b	$\Delta G(*COOH)$-f_d / $W_d^{0.5}$	0.878	0.322 eV	0.777 eV	–0.797 eV	0.391 eV
2b	$\Delta G(*N_2 \rightarrow *N_2H)$-$f_d$ / $W_d^{0.5}$	0.951	0.090 eV	0.168 eV	–0.303 eV	0.114 eV
2b	$\Delta G(*H)$-f_d / $W_d^{0.5}$	0.855	0.210 eV	0.309 eV	–0.474 eV	0.245 eV
2c	W_d-$1/(R \times S)$	0.927	0.107	0.296	–0.264	0.139
2d	f_d-n	0.995	0.012	0.019	–0.031	0.014
2g	ICOHP-ϕ_{xx}	0.885	0.188 eV	0.240 eV	–0.347 eV	0.214 eV
2g	f_d / $W_d^{0.5}$-ϕ_{xx}	0.994	0.008	0.015	–0.016	0.009
4c	$\Delta G(*OH)$-ϕ_{xy}	0.968	0.048 eV	0.108 eV	–0.093 eV	0.056 eV
4d	$-U_L(CRR)$-ϕ_{xy}	0.906	0.089 V	0.216 V	–0.212 V	0.104 V

4e	$-U_L$(NRR)-ϕ_{xy}	0.928	0.057 V	0.156 V	–0.219 V	0.074 V

Specific Comment R2-5: *It is common that there is a tradeoff between the computational dataset size and the accuracy. Guaranteeing the quality of the input dataset is vital for the effective training ML models and generating predictions with physical meanings. Specifically, for DACs containing elements like Fe, Co, and Ni, it is important to detail how the accuracy of electronic states' (doublet, triplet, etc.) collection is ensured.*

Response: We thank the reviewer for this kind reminder. We fully agree that it is necessary to correctly determine the electronic states of Fe, Co, and Ni elements in DACs, which will help us to guarantee the quality of the input dataset. To correct the magnetization, first we tested different MAGMOM, SIGMA, AMIX, and AMIX_MAG parameters in VASP. The results reveal that these parameters had little influence on the converged magnetic moments. Then we further scanned the total magnetization ranging from 0 to 6 μB for Fe, Co, and Ni-based DACs (**D. G. Vlachos** et al., *ACS Catal.* 2024, 14, 886−896), as listed in **Supplementary Table 20**. By comparing the total energies of Fe, Co, and Ni-based DACs with different total magnetic moment, we found that the X-Y sites with unspecified total magnetization are the most stable. All these results suggest that the total energies and electronic states of Fe, Co, and Ni elements is reliable in this work. One can see that Fe possesses the highest spin state (2 μ_B, triplet state), followed by Co (1 μ_B, doublet state), Ni (0 μ_B, singlet state), and other elements (0 μ_B, singlet state). The occupation of each d orbital for Fe and Co atom are listed in **Supplementary Table 21**. It shows two unpaired electrons in d_{xz} and d_{z2} orbitals of Fe atom. Furthermore, we have summarized the magnetic moment for all Fe, Co, and Ni-based X-Y sites before and after adsorption of *O, *OH and *OOH, as shown in **Supplementary Table 22**. We can find that the magnetic properties will alter when adsorbing *O, *OH and *OOH species, in line with the previous work (**K. S. Kim** et al., *Energy Environ. Sci.* 2021, 14, 3455–3468).

We have provided a description in the *Method* section:

Electronic state correction

To correct the magnetization, we tested different MAGMOM, SIGMA, AMIX, and AMIX_MAG parameters in VASP. The results reveal that these parameters had little influence on the converged magnetic moments. Then we scanned the total magnetization ranging from 0 to 6 μB for Fe, Co, and Ni-based DACs and found that the X-Y sites with unspecified total magnetization are the most stable (**Supplementary Table 20**). Fe possesses the highest spin state (2 μ_B, triplet state), followed by Co (1 μ_B, doublet state), Ni (0 μ_B, singlet state), and other elements (0 μ_B, singlet state) (**Supplementary Table 21**). The magnetic properties will alter when adsorbing *O, *OH and *OOH species, in line with the previous work[40] (**Supplementary Table 22**).

We have provided the **Supplementary Tables 20-22** in the Supplementary Information:

Supplementary Table 20. Magnetizations (μ_B) of metals with varying total magnetic moment and total energies (eV) of Fe, Co, and Ni-based DACs. '–' represents that the total magnetization is not specified during DFT calculation.

X-Y site	specified total magnetization	calculated magnetization		total energy	X-Y site	specified total magnetization	calculated magnetization		total energy
		X	Y				X	Y	
	–	2.0	2.0	-266.15		–	0.6	0.6	-263.96
	0	0.0	0.0	-265.28		0	0.0	0.0	-263.84
	1	0.8	0.9	-265.40		1	0.6	0.6	-263.96
Fe-Fe-Qv3	2	1.5	1.5	-265.65	Co-Co-Qv3	2	0.8	0.8	-263.93
	3	1.8	1.8	-265.99		3	1.0	1.0	-263.81
	4	2.0	2.0	-266.12		4	1.1	1.1	-263.28
	5	2.1	2.1	-266.12		5	1.5	1.5	-262.60
	6	2.2	2.2	-265.70		6	1.3	2.4	-261.96
	–	0.0	0.0	-261.40		–	2.1	0.0	-263.86
	0	0.0	0.0	-261.40		0	-0.8	0.1	-263.45
	1	0.1	0.1	-261.34		1	1.7	-0.1	-263.75
Ni-Ni-Qv3	2	0.3	0.3	-260.91	Fe-Ni-Qv3	2	2.0	0.0	-263.84
	3	0.6	0.6	-260.39		3	2.1	0.0	-263.82
	4	0.8	0.8	-259.73		4	2.2	0.2	-263.31
	5	1.0	1.0	-258.90		5	3.4	0.2	-262.84
	6	1.3	1.3	-258.01		6	3.5	0.3	-262.34
	–	2.0	-0.1	-265.91		–	0.7	0.0	-262.72
	0	-1.6	0.6	-265.57		0	0.3	0.0	-262.70
	1	1.9	-0.4	-265.78		1	0.8	0.0	-262.71
Fe-Ir-Qv3	2	2.0	-0.1	-265.91	Co-Ni-Qv3	2	1.0	0.1	-262.62
	3	2.1	0.2	-265.82		3	1.2	0.3	-262.11
	4	2.2	0.5	-265.64		4	1.4	0.6	-261.44
	5	2.4	0.7	-265.07		5	1.4	1.2	-260.83
	6	3.5	0.6	-264.66		6	1.6	1.2	-259.96
	–	0.8	0.0	-264.81		3	1.0	0.5	-264.46
Co-Ir-Qv3	0	0.0	0.0	-264.72	Co-Ir-Qv3	4	1.2	0.7	-263.81
	1	0.8	0.0	-264.81		5	2.3	0.7	-263.10
	2	0.9	0.3	-264.68		6	2.5	0.8	-262.43

Supplementary Table 21. 3d orbital occupations for Fe and Co elements in X-Y sites.

X-Y site	Spin	d_{xy}	d_{xz}	d_{x2-y2}	d_{yz}	d_{z2}
Fe-Fe-Qv3	up	0.77	0.90	0.62	0.89	0.69
	down	0.69	0.31	0.52	0.46	0.08
Co-Co-Qv3	up	0.84	0.80	0.65	0.81	0.48
	down	0.65	0.54	0.52	0.58	0.41

Supplementary Table 22. Magnetizations (μ_B) of metals for all Fe, Co, and Ni-based X-Y sites before and after adsorption of *O, *OH and *OOH.

X-Y site	pristine		*OOH		*O		*OH	
	X	Y	X	Y	X	Y	X	Y
Fe-Fe-Qv4	1.8	1.8	1.2	1.8	1.3	1.8	1.4	1.8

Co-Co-Qv4	0.4	0.4	0.2	0.6	2.2	0.6	0.3	0.6
Ni-Ni-Qv4	0.0	0.0	0.8	0.1	1.3	-0.1	0.8	0.1
Fe-Co-Qv4	1.8	0.5	1.2	0.6	1.3	0.5	2.0	0.4
Fe-Ni-Qv4	1.7	0.0	1.0	0.0	1.3	0.0	2.3	0.1
Fe-Rh-Qv4	1.7	0.0	1.3	0.1	1.3	0.0	2.0	0.1
Fe-Pd-Qv4	1.7	0.0	1.0	0.0	1.3	0.0	1.2	0.0
Fe-Ir-Qv4	1.8	0.1	1.3	0.2	1.3	0.1	2.0	0.1
Fe-Pt-Qv4	1.7	0.0	1.0	0.0	1.3	0.0	1.2	0.0
Co-Ni-Qv4	0.4	0.0	0.0	0.0	2.1	0.1	0.0	0.0
Co-Rh-Qv4	0.4	0.0	0.3	0.1	2.2	0.1	0.3	0.1
Co-Pd-Qv4	0.3	0.0	0.0	0.0	2.1	0.0	0.0	0.0
Co-Ir-Qv4	0.4	0.0	0.1	0.0	2.2	0.2	0.2	0.1
Co-Pt-Qv4	0.4	0.0	0.0	0.0	2.1	0.0	0.0	0.0
Fe-Fe-Qv3	2.0	2.0	1.3	2.1	1.3	2.1	2.0	1.9
Co-Co-Qv3	0.6	0.6	0.4	0.8	1.4	0.6	0.9	0.7
Ni-Ni-Qv3	0.0	0.0	0.0	0.0	1.6	0.0	0.0	0.0
Fe-Co-Qv3	2.0	0.6	1.3	0.8	1.3	0.9	2.1	0.7
Fe-Ni-Qv3	2.1	0.0	1.6	0.0	1.2	0.0	2.0	-0.1
Fe-Rh-Qv3	2.0	-0.1	1.2	-0.2	1.2	-0.1	2.1	-0.1
Fe-Pd-Qv3	2.0	0.0	0.0	0.0	1.1	0.0	1.9	0.0
Fe-Ir-Qv3	2.0	-0.1	1.6	-0.3	1.2	-0.1	2.1	-0.2
Fe-Pt-Qv3	2.0	0.0	1.7	0.0	1.1	0.0	2.0	0.0
Co-Ni-Qv3	0.7	0.0	0.1	0.0	1.3	0.0	0.0	0.0
Co-Rh-Qv3	0.8	0.0	0.0	0.0	1.4	0.0	1.3	0.1
Co-Pd-Qv3	0.6	0.0	0.2	0.0	1.2	0.0	0.1	0.0
Co-Ir-Qv3	0.8	0.0	0.0	0.0	1.5	0.1	1.3	0.1
Co-Pt-Qv3	0.6	0.0	0.1	0.0	1.2	0.0	0.0	0.0
Fe-Fe-Qv2	1.2	1.2	1.6	1.3	1.3	-1.3	1.5	1.5
Co-Co-Qv2	0.0	0.0	0.5	0.3	2.3	0.1	0.5	0.3
Ni-Ni-Qv2	0.0	0.0	0.3	0.0	1.6	0.1	0.4	0.0
Fe-Co-Qv2	1.2	0.0	1.6	0.1	1.6	0.5	1.6	0.2
Fe-Ni-Qv2	2.1	0.1	1.3	0.1	1.7	0.1	3.6	0.1
Fe-Rh-Qv2	1.2	0.0	1.6	0.0	1.2	-0.1	1.2	0.0
Fe-Pd-Qv2	0.7	0.0	1.4	0.1	1.7	0.1	1.4	0.1
Fe-Ir-Qv2	1.2	0.0	1.6	0.0	1.5	0.0	3.2	0.0
Fe-Pt-Qv2	0.0	0.0	1.3	0.1	1.7	0.1	1.4	0.1
Co-Ni-Qv2	0.8	0.1	0.0	0.0	2.4	0.2	1.0	0.2
Co-Rh-Qv2	0.0	0.0	0.6	0.1	2.3	0.0	0.7	0.1
Co-Pd-Qv2	0.8	0.1	0.0	0.0	2.5	0.1	1.0	0.1
Co-Ir-Qv2	0.0	0.0	0.6	0.1	2.3	0.0	0.7	0.1
Co-Pt-Qv2	0.8	0.2	0.9	0.2	2.5	0.2	1.0	0.2
Fe-Fe-Qv1	2.3	2.3	3.4	2.1	3.1	2.2	2.3	2.8
Co-Co-Qv1	1.2	1.2	0.1	0.0	0.4	0.3	0.1	0.3
Ni-Ni-Qv1	0.0	0.0	0.9	0.9	0.2	0.2	0.8	0.9
Fe-Co-Qv1	2.5	1.1	2.9	0.8	1.8	-0.6	3.2	0.8
Fe-Ni-Qv1	2.6	0.1	3.1	-0.3	1.6	-0.4	3.2	-0.3
Fe-Rh-Qv1	2.7	0.5	3.2	0.1	1.7	-0.1	3.3	0.1
Fe-Pd-Qv1	2.6	0.1	3.1	-0.1	1.0	-0.1	3.3	-0.1
Fe-Ir-Qv1	2.7	0.5	2.9	0.2	1.7	-0.1	3.1	0.1
Fe-Pt-Qv1	2.6	0.1	3.0	0.0	1.0	0.0	3.2	0.0
Co-Ni-Qv1	1.3	-0.1	0.9	0.0	0.7	0.4	0.8	0.1
Co-Rh-Qv1	1.6	0.5	0.6	0.0	2.3	0.2	2.2	0.1
Co-Pd-Qv1	1.3	0.1	0.9	0.0	1.0	0.0	1.8	0.0
Co-Ir-Qv1	1.6	0.5	2.0	0.1	2.2	0.2	2.2	0.1
Co-Pt-Qv1	1.3	0.1	1.4	0.0	0.1	0.0	1.9	0.0

Specific Comment R2-6: *While this work leverages descriptors and machine learning for catalyst screening, leading to the prediction and experimental validation of Co-Co/Ir-Qv3 as an optimal oxygen electrocatalyst due to its moderate ARSC value. Compared to the extensive efforts in database creation (840 catalysts), it raises the question of why further DFT analysis on this specific DAC wasn't conducted. I believe that further DFT investigations on Co-Co/Ir-Qv3 could significantly aid in uncovering its unique features that lead to superior catalytic efficiency. Such analyses would offer deeper atomic-level insights into what constitutes an "ideal" catalyst.*

Response: We thank the reviewer for this important reminder. Based on this valuable suggestion, we further investigated the electronic structure of Co-Co/Ir-Qv3. Since Co-Co/Ir-Qv3 have been screened out according to ARSC, we conducted the COHP analysis for the metal-OH bond to investigate this physical meaning of ARSC. V-V-Qv3, Ni-Ni-Qv3, Co-Co-Qv2, Co-Co-Qv4 were selected for comparison with Co-Co-Qv3 and Co-Ir-Qv3 (**Supplementary Fig. 25**). In this work, the descriptor ARSC is derived from descriptor ϕ_{xx} ($\phi_{xx} \rightarrow \phi_{xy} \rightarrow$ ARSC), which can directly quantify the effect of the d-band/FO shape of DACs on activities, that is, the position of metal-adsorbate antibonding orbitals. ARSC is inversely proportional to the antibonding position. That means a larger ARSC value corresponds to a lower antibonding position and weaker adsorption ability of adsorbates. Co atom is the main adsorption site for both Co-Co-Qv3 and Co-Ir-Qv3, of which the ARSC values are identical. As shown in **Supplementary Fig. 25**, the antibonding positions of these two DACs are relatively close, resulting in a similar ICOHP value for bond between 3d orbital of Co and O of –1.373 eV and –1.347 eV, respectively. Due to a moderate d-band width and filling of Co, the antibonding for Co-OH bond is positioned at a moderate level, while that for V-OH bond is the highest and Ni-OH is the lowest, in line with their ARSC values. When we shifted our investigation to different coordination structures, one can see that the Co-OH antibonding position for Qv3 is highest than that for Qv4, with Qv2 being the lowest. This ranking is due to the different d-band width of Co atoms governed by various coordination environments and is in line with the corresponding ARSC values. All these results indicate that Co-Co-Qv3 and Co-Ir-Qv3 are considered as the optimal candidates for oxygen electrocatalysts owing to its moderate d-band width and filling, as well as its moderate antibonding position compared with other DACs. These d-band characteristics of dual-atom sites and antibonding positions of the metal-adsorbate bond can be quickly identified using our developed ARSC values.

We have provided the statement in the manuscript *page 14*:

ARSC can directly quantify the effect of the d-band/FO shape of DACs on activities, that is, the position of metal-adsorbate antibonding orbitals. A larger ARSC value corresponds to a lower antibonding position and weaker adsorption ability of adsorbates. As shown in **Supplementary Fig. 25**, the antibonding for Co-OH bond is positioned at a moderate level on Co-Co/Ir-Qv3, while that for V-OH bond is the highest and Ni-OH is the lowest. In addition, the Co-OH antibonding position for Qv3 is highest than that for Qv4, with Qv2 being the lowest. These rankings are consistent

with the relative ARSC values, indicating that the promising performance of Co-Co/Ir-Qv3 is owing to its moderate d-band width and filling, which resulting in a moderate antibonding position.

We have provided the **Supplementary Fig. 25** in the Supplementary Information:

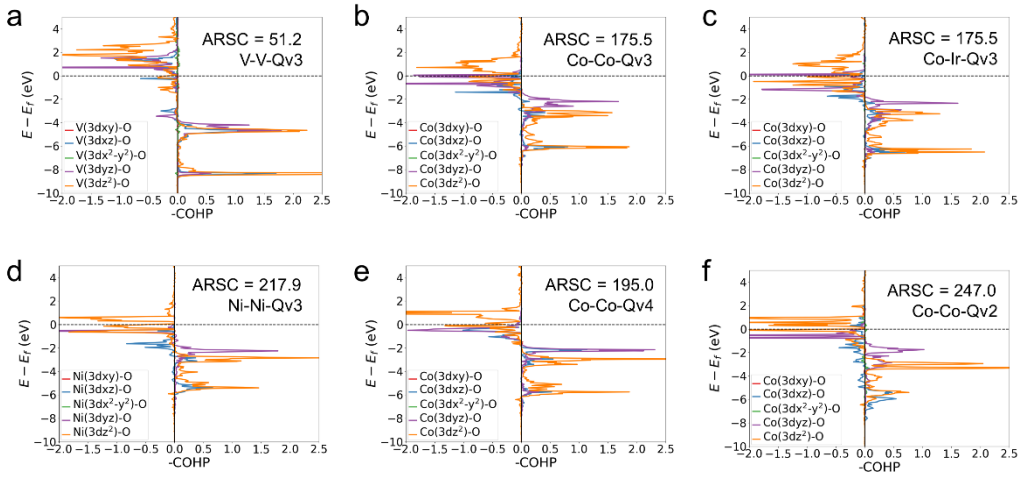

Supplementary Fig. 25. Crystal orbital Hamilton population (COHP) for metal-OH bond on DACs.

Specific Comment R2-7: *In the end of the results, the authors discussed the model's adaptability to different supports by altering the coordination from N to C and O for X-X type catalysts. While promising linear scaling relations (LSRs) are noted for OER and CRR, the model's applicability appears compromised for NRR over X-Y type catalysts, as evidenced by deteriorating scaling and notable outliers in Fig. S31 (R2 is also missing), indicating the model's limitations in more complex coordination environments. Therefore, it's crucial that the authors address the potential limitations, shortcomings, or areas for refinement when applying their approach to more intricate DACs that utilize non-uniform supports, with a few sentences in the conclusion.*

Response: We are very grateful to the reviewers for this kind concern. We fully agree that this descriptor may have potential limitations when applied to substrates outside of the graphene which we discussed in this paper. We believe that the occurrence of individual outliers shown in **Supplementary Fig. 51** (Supplementary Fig. 31 in our previous submission) stems from the absence of 2D expanded phthalocyanine as substrates in our database when developing the descriptor. As displayed in **Supplementary Figs. 49 and 50**, our developed descriptor presents remarkable prediction accuracy for ORR/OER/CRR, in which the N coordination is replaced by other elements, but the graphene substrate remains the same. In contrast, due to the substitution of graphene substrate with 2D expanded phthalocyanine, the microenvironment of the dual-atom sites undergoes slight changes, resulting in a decline in the descriptor's ability to accurately describe activity (**Supplementary Fig. 51**). Another reason for the appearance of outliers is that all data in this figure are sourced from previously reported literature instead of the uniform calculations in this

work. Since the computed activity strongly depends on the selection of VASP parameters as well as the construction of atomic models, variations in results may occur across different works. Despite three DACs deviating from the LSR (VCr, TiV, TaTi), our proposed descriptor can still effectively predict the activity of the majority of DACs with **R^2 = 0.80 (we have revised the Supplementary Fig. 51 with R^2 value)**. It is worth noting that a few outliers fail to affect the catalyst screening results guided by the descriptor. One can see that the DACs exhibiting the highest NRR activity, such as MoV, do present the lowest ϕ_{xy} value. It means that the optimal catalysts can still be successfully, quickly, and correctly identified via our developed descriptor.

We can conclude that since our constructed descriptor cannot accurately capture the impact of substrates outside of graphene on the microenvironment of dual-atom sites, there will be certain limitations when the descriptor is applied to other substrates and some outliers may occur. However, considering that atomic effects, synergistic effects, and reactant effects on DACs are not altered by different substrates, our developed descriptor can still reflect the activity trends on other substrates to a certain extent. For example, the descriptor has been verified that it can still be applied to 2D expanded phthalocyanine to quickly screen out efficient catalysts, such as MoV, although there are a few outliers. **Although our developed descriptor has exhibited high universality, for future high-throughput screening of DACs on other substrates, it would be better to further optimize the descriptor based on the characteristics of different substrates to enhance the whole prediction accuracy.**

We have provided the statement in the manuscript *page 17*:

In addition, using reported data, a linear relationship between U_L(NRR) for X-Y sites supported on 2D expanded phthalocyanine and ϕ_{xy} can be plotted[42], where the ideal DACs, such as MoV, can be quickly identified by our descriptor **(Supplementary Fig. 51**). However, we also notice individual outliers, suggesting that the potential limitation of our constructed descriptor is that the impact of substrates outside of graphene on the microenvironment of dual-atom sites is not considered in this work. It should be known that, although the descriptor ARSC has been demonstrated to possess the capability to unveil the structure-activity relationships across various dual-atom systems and reactions, for future high-throughput screening of DACs on other substrates, it would be better to further optimize this descriptor based on the characteristics of different substrates to enhance the whole prediction accuracy. This insight will enhance the future potential of our descriptor.

We have updated the **Supplementary Fig. 51** and added R^2 in the Supplementary Information:

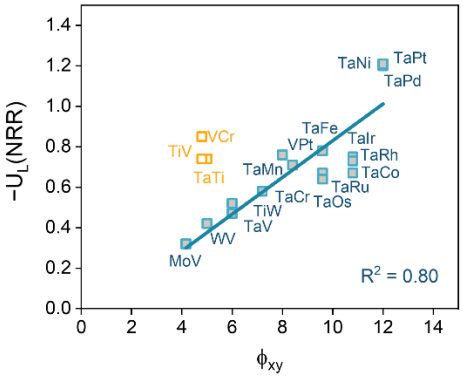

Supplementary Fig. 51. U_L(NRR) as a function of ϕ_{xy} on X-Y sites supported on 2D expanded phthalocyanine. Data are taken from the reported works[2].

Specific Comment R2-8: *I highly recommend incorporating a comprehensive workflow diagram detailing the entire project, which should cover dataset construction, descriptor refinement, ML prediction, and experimental validation processes. Additionally, including a table that lists all symbols used along with their physical meanings would greatly enhance the manuscript's readability. Also, it is weird to plot the volcano curve with a V-shape by using "-UL" in Fig. S1 and S2.*

Response: We appreciate the reviewers for this important reminder. We have provided such a workflow diagram, which including dataset construction, descriptor refinement, ML prediction, and experimental validation in **Fig. 1**. In addition, according to your kind reminder, we have listed all symbols and their physical meanings in **Supplementary Table 24**. We also revised **Supplementary Figs. 1 and 2** by adjust the $-U_L$ to the common U_L.

We have provided the **Fig. 1** in the manuscript:

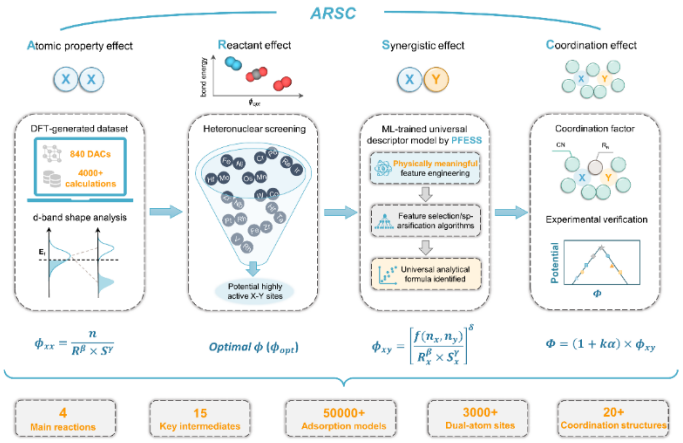

Fig. 1 | General workflow of our work. It includes four major parts: i) primitive descriptor (ϕ_{xx}) for atomic property effects through d-band shape analysis, ii) screening principle (ϕ_{opt}) of potential desirable heteronuclear DACs based on reactant

effects, iii) ML-based descriptors (ϕ_{xy}) for synergistic effects through physically meaningful feature engineering based on ϕ_{xx} and feature selection/sparsification algorithms, iv) the final universal descriptor model (Φ) with quantification of coordination effects and corresponding experimental verifications.

We have provided the **Supplementary Table 24** in the Supplementary Information:

Supplementary Table 24. The physical meaning of all symbols mentioned in this work.

Symbol	Physical meaning
DACs	dual-atom catalysts
SACs	single-atom catalysts
ORR, CRR, NRR	O_2, CO_2, and N_2 reduction reactions
OER	oxygen evolution reaction
machine learning	ML
Φ/ARSC	the universal descriptor, which captures the atomic property, reactant, synergistic, and coordination effects of DACs
ϕ_{xx}	primitive descriptor for X-X sites
ϕ_{opt}	the optimal ϕ_{xx} value for different reactions and products
ϕ_{xy}	descriptor for X-Y sites
PFESS	our developed physically meaningful feature engineering and feature selection/sparsification method
X-X	homonuclear dual-atom sites
X-Y	heteronuclear dual-atom sites, where X is defined as the main metal that binds the adsorbate
Qv1, Qv2, Qv3, Qv4	different coordination structures
XX@N3A6	N presents the coordination number of N atoms for each metal atom, and A presents the actual number of N atoms that can coordinate to the entire X-X site
ΔG(*OH)	the adsorption free energies of *OH
ΔG(*OH) on X-X sites	the average value of ΔG(*OH) on X-X-Qv1, X-X-Qv2, X-X-Qv3, and X-X-Qv4
ΔG(z)	the adsorption free energies of z, z represents *OH, *COOH, or $*N_2 \rightarrow *N_2H$.
$\Delta G_{opt}(z)$	the optimal value of ΔG(z), which is located near the top of the U_L-ΔG(z) volcano plot
U_L	limiting potential
FO	frontier orbital
f_d	d-band filling
W_d	d-band width
f_{FO}	FO filling
W_{FO}	FO width
n	valence electron number
R	atomic radius
S	the number of electron shells
β	non-negative index of R
γ	non-negative index of S
$d_{M\text{-}M}$	metal-metal bond distance
ICOHP	integrated crystal orbital Hamilton population
n_x, n_y	valence electron number for X- or Y-metals at X-Y sites
R_x, R_y	atomic radius for X- or Y-metals at X-Y sites
S_x, S_y	the number of electron shells for X- or Y-metals at X-Y sites
δ	index in the function of ϕ_{xy}

$f(n_x, n_y)$	the absolute differences or divisions on n_x and n_y
CN	the N coordination number of each metal atom
R_N	the ratio of N atoms simultaneously bonded to two metals
λ	index in the function of α
N_m	the maximum number of N atoms that can coordinate to the entire X-Y site for a specific CN ($2 \times CN$)
N_a	the actual number of N atoms that coordinate to the entire X-Y site
α	coordination factor
$\overline{W_d}$	averaged W_d for all metals in a certain coordination structure
k	the coefficient for α in the function of Φ
LSRs	linear scaling relations
$E_{1/2}$	half-wave potential
η_{10}	overpotential at a current density of 10 mA cm^{-2}

We have updated the **Supplementary Figs. 1 and 2** in the Supplementary Information:

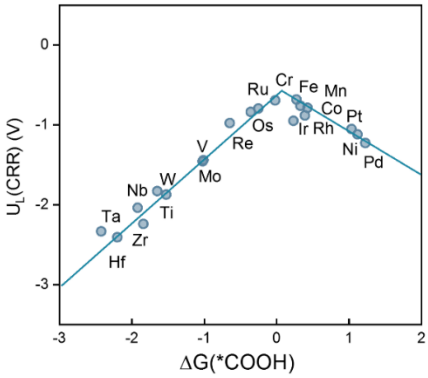

Supplementary Fig. 1. Volcano plot for U_L(CRR) towards CO/CH_4/CH_3OH versus ΔG(*COOH) on X-X sites.

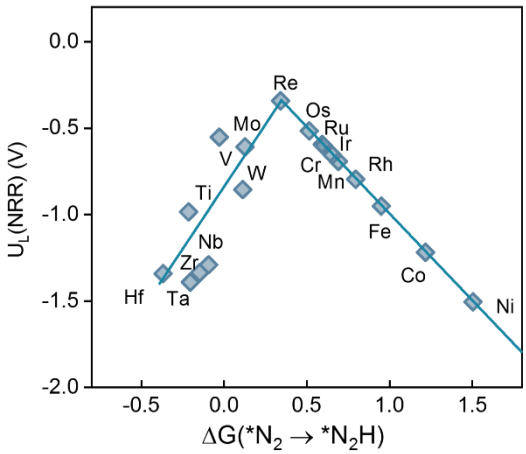

Supplementary Fig. 2. Volcano plot for U_L(NRR) towards NH_3 versus ΔG(*N_2 → *N_2H) on X-X sites.

Specific Comment R2-9: *Throughout the manuscript and SI, there's a noticeable absence of detailed descriptions regarding the DFT models, aside from the simplified local configurations depicted in figures and a brief mention of using a monolayer graphene as the support. Moreover, the Python codes utilized in the analysis have not been shared. This omission makes it almost impossible to ensure the reproducibility of this work. To address this issue and support the growing DAC community, particularly those focused on electrocatalytic reactions, and to keep with the journal's open-source ethos, it is strongly recommended/encouraged that the configurations be provided in commonly used formats such as VASP (POSCAR, CONTCAR) or extended XYZ. These files should be zipped and included as supporting information and the Python codes should be uploaded to platforms like GitHub. Making these details resources readily accessible, rather than "upon request", ensures that other researchers can replicate the study's findings and apply the configurations to their own work, fostering further advancements in this field.*

Response: We thank the reviewer for this kind reminder. We have provided the atomic coordinates of the optimized model (CONTCARs), which including multiple configurations of DACs we discussed in this work, as a separate Supplementary Data 1. Moreover, the Python code written to perform PFESS method and train universal descriptors, has been open-sourced under the Apache 2.0 license and is accessible via our GitHub repository at https://github.com/TJU-ECAT-AI/PFESS. We will continue to improve the openness of raw data and the construction of the DAC database until our work is published.

Reviewer #3:

General Comments R3: *In this paper, X. Lin et al. presents a novel interpretable descriptor model, called ARSC, which integrates activity and selectivity prediction across multiple electrocatalytic reactions (such as O2/CO2/N2 reduction and O2 evolution reactions). ARSC relies solely on easily accessible intrinsic properties and effectively disentangles atomic properties, reactants, synergistic effects, and coordination influences on the d-band shape of dual-atom sites. It is developed through a physically meaningful feature engineering and selection/sparsification (PFESS) method. By leveraging ARSC, optimal catalysts for various products can be rapidly identified without resorting to over 50,000 density functional theory calculations. The universality of the model is confirmed through extensive validation against existing literature and subsequent experiments, which pinpoint Co-Co/Ir-Qv3 as top bifunctional oxygen reduction and evolution electrocatalysts.*

Unfortunately, I have several critical concerns, which should be properly clarified before I agree to the publication of this manuscript.

Response: Many appreciations to the reviewer for the careful review of our manuscript. The constructive concerns provided have been invaluable in enhancing the quality of our work. We deeply appreciate the opportunity to address these insightful questions. Each of your comments has been carefully considered, leading us to enhance our manuscript by incorporating detailed explanations and improvements across all the points you raised.

Specific Comment R3-1: *While the target catalyst or products may differ from those in previous reports, it's worth noting that descriptor-based approaches have been published several times before. Could you please discuss these papers and the differences with them?*

a) Nat. Commun. 14, 4449 (2023)

b) Nat. Nanotech. 17, 606–612 (2022)

c) J. Mater. Chem. A,10, 1451-1462 (2022)

d) Nat. Commun. 12, 1833 (2021)

e) J. Phys. Chem. Lett. 11, 3481–3487 (2020)

Response: We thank the reviewer for this kind reminder. Please allow us to explain the differences between these papers mentioned above and this work, which will include three aspects, namely target, practical utility, and universality, as shown in **Supplementary Fig. 52 and Table R3-1-1**. Compared with other descriptors, our developed descriptor can predict both experimental and theoretical results simultaneously. It is composed of intrinsic properties of active sites and enables low-cost, rapid, and high-throughput screening of catalysts. **The most unique aspect of**

our descriptor lies in its ability to unify multiple electrocatalytic reactions, which has not been achieved by other descriptors yet.

Table R-3-1-1. Difference of descriptors between previous papers and this work. '–' represents that this item cannot be evaluated, as the descriptor is not an intrinsic descriptor.

Paper	Target		Practical utility	Universality			
	Experimental value	Theoretical value	Intrinsic (linked with target)	Metal effect	Synergistic effect	Coordination effect	Multiple reactions
This work	√	√	√	√	√	√	√
A	×	√	×	–	–	–	–
B	√	×	×	–	–	–	–
C	×	√	√	√	√	×	×
D	×	√	√	√	×	√	×
E	×	√	×	√	×	×	×

First is the difference in the prediction targets of the descriptors. As prediction targets, the catalytic performance can be classified into three categories: stability, selectivity, and activity. It seems that most papers focus more on activity descriptor (Paper A, B, D, E, and this work). The descriptor proposed by this work can also reflect the selectivity towards different products and reactions of DACs. In Paper B, the descriptor for stability, selectivity, and activity are all considered, making the evaluation towards catalysts more comprehensive. Experimental or theoretical value is another kind of prediction targets. Using experimental values as prediction targets, like paper B, would make the conclusions more realistic and reliable, avoiding errors introduced by DFT calculations. However, the high cost of acquiring experimental data will hinder the efficiency of high-throughput screening of catalysts. Considering this factor, DFT calculations can significantly save costs, thus the corresponding descriptors have been widely used in catalyst design within complex system (Paper A and C-E). The descriptors proposed by this work can predict not only theoretical but also experimental catalytic performance. Using theoretical values as the training set, the descriptor ARSC exhibit a high universality for over 50000 adsorption models. Moreover, the reliability of ARSC has been experimentally validated by 28 reported works and our subsequent experiments, that means the different structure-performance relationships of DACs reported by multiple previous works can be unified by this work.

Second, the practical utility can be assessed through the type of descriptors. According to the different types, the descriptor can be classified into three categories, namely energy-based, electronic, and intrinsic descriptors (**Supplementary Fig. 52**). Energy-based descriptors, such as the adsorption energies of the key intermediates, are essential in determining the underlying mechanism, often directly related to catalytic performance. This type of descriptor is commonly used in catalyst screening, such as Paper A and B. However, energy-based descriptors often lack some insightful information about the structure-performance relationship from the perspective of the electronic orbital and geometry. To address this issue, electronic descriptors have been

developed correspondingly. For example, the d-band model, such as the d-band center, has been particularly successful in clarifying the trends of adsorption abilities (Paper A and D). Nevertheless, although the energy-based and electronic descriptors have achieved great success in describing catalytic performance, their computationally costly and experimentally unobtainable properties limit the understanding of the structure-performance relationship to a case-by-case basis. Since DFT values are unknown beforehand and vary with different methodologies, it significantly limits the practical applicability of those descriptors in directly designing new materials (**D. Morgan** et al., *Chem. Mater.* 2019, 31, 785–797). In order to maximize descriptor usability, an optimal descriptor should be easily obtainable and provide physical insight, which has potential to achieve the low-cost, quick, and high-throughput screening of new effective catalysts (**W. Yin** et al., *Nat. Commun.* 2020, 11, 3513). In this situation, intrinsic descriptors, which consists of the intrinsic properties of elements and geometric structures of active sites, are perfectly suitable. The descriptor expression in Paper D is formed by the electronic and intrinsic descriptors together, which may increase the cost. The intrinsic descriptors can also be divided into two types. Some works use energy-based descriptors as the intermediary to correlate intrinsic descriptors with catalytic performance (Paper E). The prediction accuracy and utility of this intrinsic descriptor would be lower due to the presence of prediction errors between catalytic performance and energy-based descriptors as well. As a result, from the aspect of the practical utility, the more perfect one is to directly link with the catalytic performance (Paper C and this work).

Finally, we will further discuss the difference in the universality of intrinsic descriptors between papers mentioned above. A descriptor that can decouple and quantify more effects of active sites on catalytic performance would exhibit higher universality. For a single-atom site, it includes the metal effect (atomic properties of the metal center) and the coordination effect. For a dual-atom site, an additional synergistic effect (metal-metal interaction) also needs to be contained. As shown in **Table R3-1-1**, only the descriptor proposed in this work quantifies all these three effects simultaneously, showing a superior universality for the clarification of the structure-performance relationship of DACs. More importantly, this descriptor successfully unified multiple electrocatalytic reactions, breaking the limitations of traditional descriptors for describing individual reactions.

In conclusion, by comparing this work with other papers, we concluded that our proposed descriptor has an advantage in terms of reliability, practicality, and universality. This descriptor shows a comprehensive design principle, which significantly accelerates the high-throughput screening of electrocatalysts towards multiple products with low cost. It makes our understanding of the structure-performance relationship of DACs more deeply.

We have provided the statement in the *Introduction* section:

Nowadays, numerous notable descriptors have been reported, effectively revealing the structure-performance relationship on SACs or DACs[14-18]. However, when

considering their reliability, practical utility, and universality comprehensively, the optimal low-cost descriptor capable of unifying multiple reactions while addressing both experimental and theoretical results remains elusive.

14. Fang, C. et al. Synergy of dual-atom catalysts deviated from the scaling relationship for oxygen evolution reaction. *Nat. Commun.* **14**, 4449 (2023).

15. Kaiser, S. K. et al. Performance descriptors of nanostructured metal catalysts for acetylene hydrochlorination. *Nat. Nanotechnol.* **17**, 606-612 (2022).

16. Li, D., Xu, H., Zhu, J. & Cao, D. Fast identification of the stability of atomically dispersed bi-atom catalysts using a structure descriptor-based model. *J. Mater. Chem. A* **10**, 1451-1462 (2022).

17. Han, Z. K. et al. Single-atom alloy catalysts designed by first-principles calculations and artificial intelligence. *Nat. Commun.* **12**, 1833 (2021).

18. Yuan, H., Li, Z., Zeng, X. C. & Yang, J. Descriptor-based design principle for two-dimensional single-atom catalysts: carbon dioxide electroreduction. *J Phys Chem Lett* **11**, 3481-3487 (2020).

We have provided the **Supplementary Fig. 52** in the Supplementary Information:

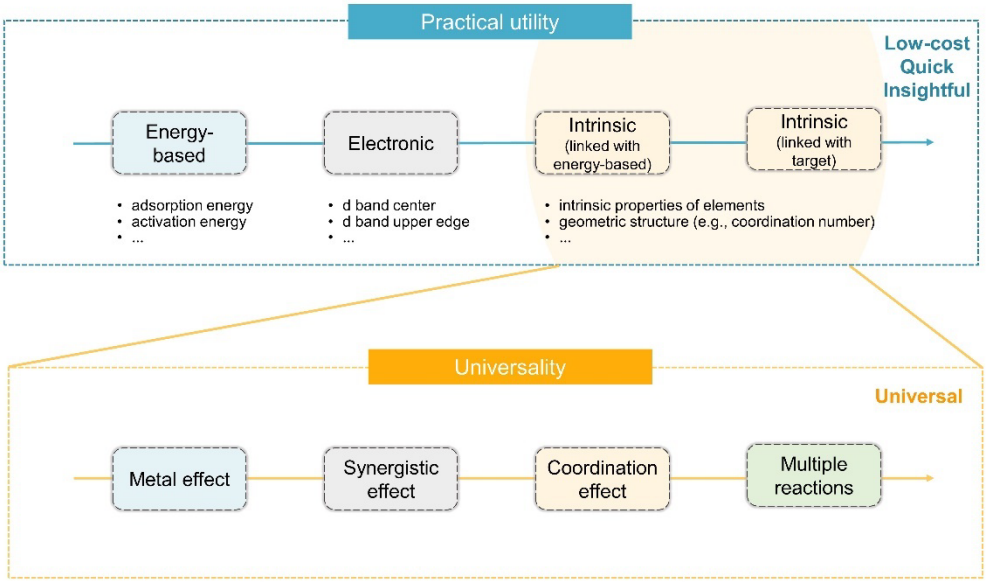

Supplementary Fig. 52. Schematic diagram of the classification and evaluation for descriptors.

Specific Comment R3-2: *I believe that the efficiency of the catalyst is not significantly superior compared to other catalysts, and it is important to provide more detailed information. As the author suggested in Supplementary Table 11, various previous ORR catalysts are listed. However, the level of detail provided is not sufficient for a reasonable comparison. The concentration of electrolyte, pH, substrate, and other relevant parameters should be tabulated and compared with other catalysts.*

Response: We are very grateful to the reviewers for your kind reminder. We have incorporated more details in **Supplementary Table 15** (Supplementary Table 11 in our previous submission), including electrolyte, pH, substrate, and the loading of metals.

We have updated the **Supplementary Table 15** in the Supplementary Information:

Supplementary Table 15. ORR activity comparison of Co-Co/Ir-NC with the state-of-the-art DACs reported recently. To ensure consistent experimental conditions, all electrolytes in these works are KOH. The symbol '–' represents that the specific values have been not mentioned in the paper.

X-Y dual-atom sites	Electrocatalyst	$E_{1/2}$ (*vs.* RHE)	Loading (wt.%) X/Y	Substrate	Electrolytes	pH	Ref.
CoCo@N3A7	Co-Co-NC	0.941	2.2	N-doped carbon	0.1 M KOH	12.9	This work
CoIr@N3A7	Co-Ir-NC	0.937	1.3/1.0	N-doped carbon	0.1 M KOH	12.9	This work
	FeNi SAs/NC	0.84	1.83/1.63	N-doped carbon	0.1 M KOH	12.7~13	3
FeNi@N3A6	Fe-NiNC-50	0.85	0.33/0.57	N-doped carbon	0.1 M KOH	12.7~13	4
	$Ni_{66}Fe_{34}$-NC	0.85	0.48/0.93	N-doped carbon	0.1 M KOH	12.7~13	5
FeZn@N3A6	Fe-Zn-SA/NC	0.85	0.22/0.10	N-doped carbon	0.1 M KOH	12.7~13	6
	FeCo-NC	0.877	0.339/0.981	N-doped carbon	0.1 M KOH	12.7~13	7
FeCo@N3A6	f-FeCoNC	0.89	–	N-doped carbon	0.1 M KOH	12.7~13	8
	f-FeCo-CNT	0.87	3.51/2.43	N-doped carbon nanotubes	0.1 M KOH	12.7~13	9
	(Fe,Co)/CNT	0.954	1.21/1.13	N-doped carbon nanotubes	0.1 M KOH	12.7~13	10
MnFe@N4A6	FeMn-DSAC	0.922	0.64/1.05	N-doped carbon nanosheets	0.1 M KOH	12.7~13	11
	Fe,Mn/N–C	0.928	1.6/2.3	N-doped carbon	0.1 M KOH	12.7~13	12
FeCo@N4A8	FeCo-ISAs/CN	0.92	0.964/0.218	N-doped carbon	0.1 M KOH	12.7~13	13
	FeCo-DACs/NC	0.877	0.76/0.80	N-doped carbon	0.1 M KOH	12.7~13	14
	Fe,Co,N−C	0.90	1.06/0.77	N-doped carbon	0.1 M KOH	12.7~13	15
	FeCo-IA/NC	0.88	0.26/1.06	N-doped carbon	0.1 M KOH	12.7~13	16
	Fe/Ni-N_x/OC	0.938	1.35/0.47	N-doped carbon	0.1 M KOH	12.7~13	17
FeNi@N4A8	FeNi/NC	0.89	1.92/0.55	Ketjenblack Phenanthroline	0.1 M KOH	12.7~13	18
	FeNi-SAs@NC	0.89	0.21/0.24	N-doped carbon	1 M KOH	13.7~14	19
FePt@N4A8	Fe-N_4/Pt-N_4@NC	0.93	1.12/0.45	N-doped carbon	0.1 M KOH	12.7~13	20
CoIr@N3A5	IrCo−N−C	0.911	1.02/0.18	N-doped carbon	0.1 M KOH	12.7~13	21
CoNi@N4A8	NiCo DASs/N-C	0.88	0.43/0.37	N-doped carbon	0.1 M KOH	12.7~13	22
CoZn@N4A8	ZnCo-NC-II	0.86	1.43/1.41	N-doped carbon	0.1 M KOH	12.7~13	23
FeIr@N4A6	IrFe−N−C	0.92	0.19/0.14	N-doped carbon	1 M KOH	13.7~14	24

FeZn@N4A6	Fe/Zn–N–C	0.906	4.68/3.37	N-doped carbon	0.1 M KOH	12.7~13	[25]
	CoFe−N−C	0.897	–	N-doped carbon	0.1 M KOH	12.7~13	[26]
FeCo@N4A6	Fe/Ni(1:3)-NG	0.842	1.19/0.94	N-doped graphene	0.1 M KOH	12.7~13	[27]
	Fe/Ni–N–C	0.861	0.56/1.2	N-doped carbon	0.1 M KOH	12.7~13	[28]
	Fe,Ni/N-C@NG	0.858	–	N-doped graphene nanosheets	0.1 M KOH	12.7~13	[29]
CoZn@N4A6	ZnCo-HNC	0.82	–	N-doped carbon	0.1 M KOH	12.7~13	[30]

* For some studies, the pH was not specified, so we provided a reasonable range.

Specific Comment R3-3: *For reproducibility, the error bars should be accurately expressed in the data, including overpotential.*

Response: Many appreciations to the reviewer for this important suggestion. To verify the reproducibility of the overpotentials we proposed, we have carried out triplicate reproducibility experiments for both ORR and OER activities on Co-Co-NC and Co-Ir-NC, as displayed in **Supplementary Figs. 42 and 45**. We have found that the polarization curves of each catalyst sample in three different tests remain the same. **The standard deviation (SD) is within 1.5 mV for both $E_{1/2}$ and η_{10} values, indicating good reproducibility of the activity data in this work**. We have added the error bars for Co-Co-NC and Co-Ir-NC in **Fig. 5i**. The error bars for other DACs were not added because these papers did not report the corresponding data due to their minimal SD of ORR/OER activity. In addition, we have noticed that the error bar in **Fig. 5h** represents the differences in $E_{1/2}$ between multiple works with the same dual-atom site, not different $E_{1/2}$ values within the same work. Due to our oversight, this meaning of error bars in **Fig. 5h** was not conveyed in the previous submission. We deeply apologize for any misunderstanding caused by this mistake.

We have updated the **Fig. 5i** in the manuscript:

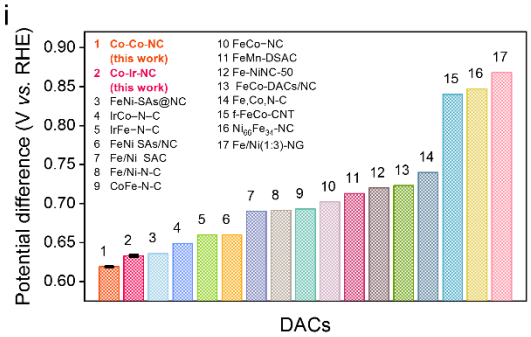

Fig. 5i. ORR and OER bifunctional activity comparisons between Co-Co/Ir-NC and other representative DACs (**Supplementary Table 17**).

We have provided the statement in the title of **Fig. 5h**:

The error bar represents the differences in $E_{1/2}$ between multiple works with the same dual-atom site.

We have provided the **Supplementary Figs. 42 and 45** in the Supplementary Information:

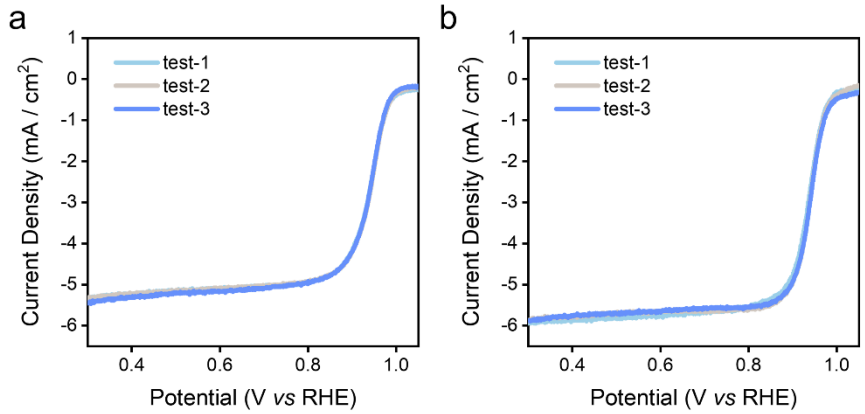

Supplementary Fig. 42. ORR polarization curves of **a** Co-Co-NC and **b** Co-Ir-NC in triplicate reproducibility tests.

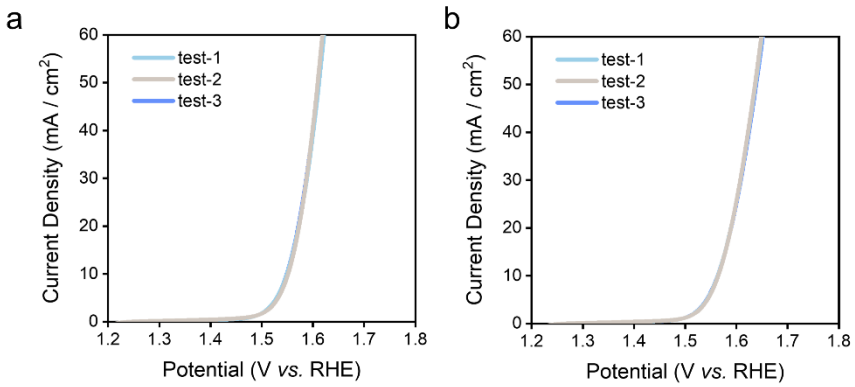

Supplementary Fig. 45. OER polarization curves of **a** Co-Co-NC and **b** Co-Ir-NC in triplicate reproducibility tests.

Specific Comment R3-4: *One of the key factors to consider is the degradation of catalysts. Although the overpotential is much lower, if the duration is not sufficient, the catalyst may be difficult to consider as a superior catalyst. Could you please suggest including cycling or duration data in detail and comparing it to other reported catalysts?*

Response: We thank the reviewer for this kind reminder. We have comprehensively conducted the stability test of Co-Co/Ir-NC for both ORR and OER. The ORR stability was evaluated by the accelerated stress test (AST) in the potential range of 0.6~1.0 V *vs.* RHE with the scan rate at 50 mV s^{-1} for continuous 10000 cycles in oxygen-saturated 0.1 M KOH solution. **Supplementary Fig. 44** displays only 7 mV and 5 mV negative shifts of $E_{1/2}$ for Co-Co-NC and Co-Ir-NC, respectively, which is comparable and even better than other reported carbon-based DACs (**Supplementary Table 16**), suggesting reasonably high catalytic stability. The OER stability was investigated using chronoamperometry measurements at a constant current density of

10 mA cm^{-2}. As shown in **Supplementary Figs. 47 and 48**, the remarkable activities of Co-Co/Ir-NC can be well maintained at 10 mA cm^{-2} for 200 h with minimal degradation, demonstrating superior stability of our designed DACs compared to other reported carbon-based DACs (**Supplementary Table 18**).

We have provided the statement in the manuscript *page 17*:

Slightly negative shifts of $E_{1/2}$ are observed after 10,000 cycling for Co-Co/Ir-NC, suggesting reasonably high catalytic stability compared with other DACs (**Supplementary Fig. 44 and Supplementary Table 16**).

Co-Co/Ir-NC can be well maintained at 10 mA cm^{-2} for 200 h with minimal degradation, demonstrating superior stability compared to other carbon-based DACs (**Supplementary Figs. 47 and 48 and Supplementary Table 18**).

We have provided the statement in the *Method* section:

The ORR stability was evaluated by the accelerated stress test (AST) in the potential range of 0.6~1.0 V *vs.* RHE with the scan rate at 50 mV s^{-1} for continuous 10000 cycles in oxygen-saturated 0.1 M KOH solution. The OER stability was investigated using chronoamperometry measurements at a constant current density of 10 mA cm^{-2}.

We have provided the **Supplementary Figs. 44 and 47-48** in the Supplementary Information:

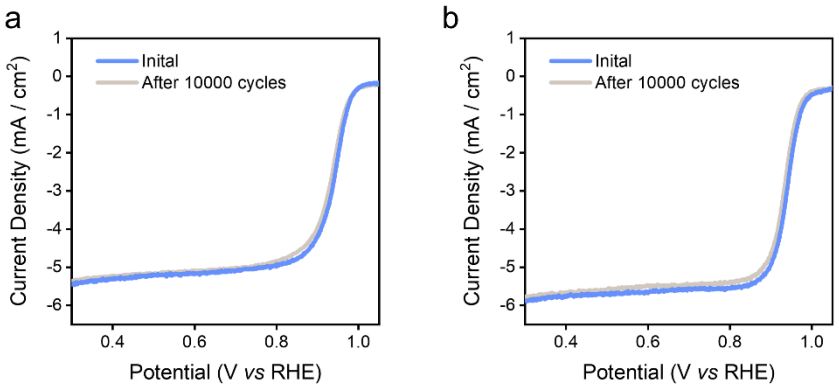

Supplementary Fig. 44. ORR polarization curves of **a** Co-Co-NC and **b** Co-Ir-NC before and after 10,000 potential cycles.

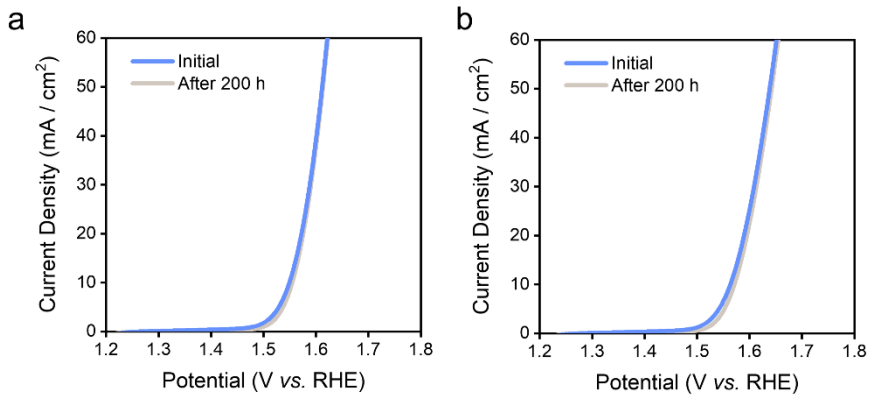

Supplementary Fig. 47. OER polarization curves of **a** Co-Co-NC and **b** Co-Ir-NC before and after 200-h-long working at 10 mA cm^{-2}.

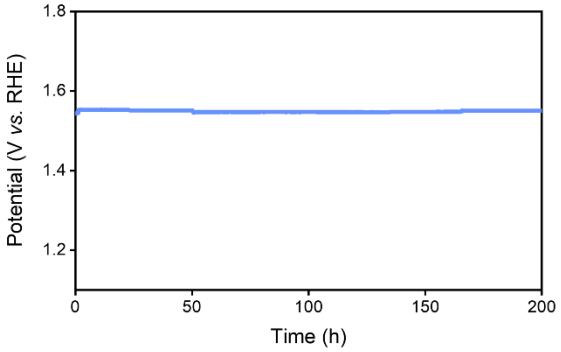

Supplementary Fig. 48. Chronopotentiometric curves of Co-Co-NC at a constant current density of 10 mA cm^{-2}.

We have provided the **Supplementary Tables 16 and 18** in the Supplementary Information:

Supplementary Fig. 16. ORR stability comparison of Co-Co/Ir-NC with carbon-based DACs reported recently. The symbol '–' represents that the specific values have been not mentioned in the paper.

Electrocatalyst	Electrolytes	Cycle number	$E_{1/2}$ shift (mV *vs.* RHE)	Ref.
Co-Co-NC	0.1 M KOH	10000	7	This work
Co-Ir-NC	0.1 M KOH	10000	5	This work
Fe-NiNC-50	0.1 M KOH	5000	9	4
Fe-Zn-SA/NC	0.1 M KOH	5000	–	6
(Fe,Co)/CNT	0.1 M KOH	10000	–	10
FeMn-DSAC	0.1 M KOH	10000	5	11
Fe,Mn/N–C	0.1 M KOH	40000	–	12
FeCo-ISAs/CN	0.1 M KOH	4000	–	13
Fe/Ni-N_x/OC	0.1 M KOH	5000	–	17
FeNi/NC	0.1 M KOH	3000	10	18
FeNi-SAs@NC	1 M KOH	1000	6	19
Fe-N_4/Pt-N_4@NC	0.1 M KOH	10000	8	20

IrCo−N−C	0.1 M KOH	10000	10	[21]
NiCo DASs/N-C	0.1 M KOH	5000	–	[22]
ZnCo-NC-II	0.1 M KOH	10000	3	[23]
IrFe−N−C	1 M KOH	5000	5	[24]
Fe/Ni(1:3)-NG	0.1 M KOH	3000	23	[27]
Fe,Ni/N-C@NG	0.1 M KOH	5000	3	[29]
ZnCo-HNC	0.1 M KOH	2000	18	[30]

Supplementary Fig. 18. OER stability comparison of Co-Co/Ir-NC with carbon-based DACs reported recently. The symbol '–' represents that the specific values have been not mentioned in the paper.

Electrocatalyst	Electrolytes	Durability time	η_{10} shift [activity loss]	Ref.
Co-Co-NC	1 M KOH	200 h	6 mV	This work
Co-Ir-NC	1 M KOH	200 h	8 mV	This work
FeN_4B-NiN_4B	0.1 M KOH	2000 cycles	10 mV	[31]
FeN_4-SC-NiN_4	0.1 M KOH	5000 cycles	9 mV	[32]
FeNi SAs/NC	0.1 M KOH	35 h	–	[3]
Fe-NiNC-50	1 M KOH	1500 cycles	2	[4]
$Ni_{66}Fe_{34}$-NC	0.1 M KOH	10000 s	[10.7%]	[5]
FeCo-NC	0.1 M KOH	5000 cycles	–	[7]
f-FeCo-CNT	0.1 M KOH	3000 cycles	10	[9]
FeNi-SAs@NC	1 M KOH	10 h/1000 cycles	–	[19]
IrCo−N−C	0.1 M KOH	2000 cycles	–	[21]
IrFe−N−C	1 M KOH	400 h	–	[24]
CoFe−N−C	1 M KOH	25 h	[3.4 %]	[26]
Fe/Ni(1:3)-NG	0.1 M KOH	1000 cycles	–	[27]

Specific Comment R3-5: *The author primarily focused on suggesting the thermodynamic overpotential without addressing kinetics, except for the experimental Tafel plot in Supplementary Fig. 27. It would be beneficial to include kinetics barriers by employing (CI)-NEB methods.*

Response: We thank the reviewer for your crucial comment. We have calculated the kinetics barriers on Co-Y-Qv3 (Y = Co, Ir, Ni, Rh, Pd, Pt) due to their superior ORR activity thermodynamically identified by this work. Utilizing CI-NEB methods, the kinetic process of four pathways, including the O_2 hydrogenation, dissociation of *OOH, *OH formation, and second H_2O formation were comprehensively investigated on Co-Co-Qv3 and Co-Ir-Qv3 (**Supplementary Figs. 22 and 23**). We found that these two DACs possess low reaction barriers with that of 0.34 and 0.36 eV, respectively, suggesting a reasonable reaction rate at room temperature. The dissociation of *OOH is identified as the rate-determining step, in line with previous literature (**S. Lin** et al., *J. Catal.* 2021, 396, 215–223). As a result, by further accessing the kinetics barriers of the *OOH dissociation, our calculations suggest that Co-Ni-Qv3, Co-Rh-Qv3, Co-Pd-Qv3 and Co-Pt-Qv3 can also overcome kinetic obstacles (0.34, 0.39, 0.37, and 0.36 eV, respectively) (**Supplementary Figs. 24**). All

these results illustrate that our identified DACs with favorable thermodynamic behavior also exhibit favorable kinetic behavior.

We have provided the statement in the manuscript *pages 13-14*:

To further investigate whether these high-active DACs will be blocked by severe kinetic issues, we calculate the kinetics barriers on Co-Y-Qv3 (Y = Co, Ir, Ni, Rh, Pd, Pt), and find that all the Co-Y-Qv3 can overcome kinetic obstacles with energy below 0.4 eV, exhibiting favorable kinetic behavior. (**Supplementary Figs. 22-24**).

We have provided the **Supplementary Figs. 22-24** in the Supplementary Information:

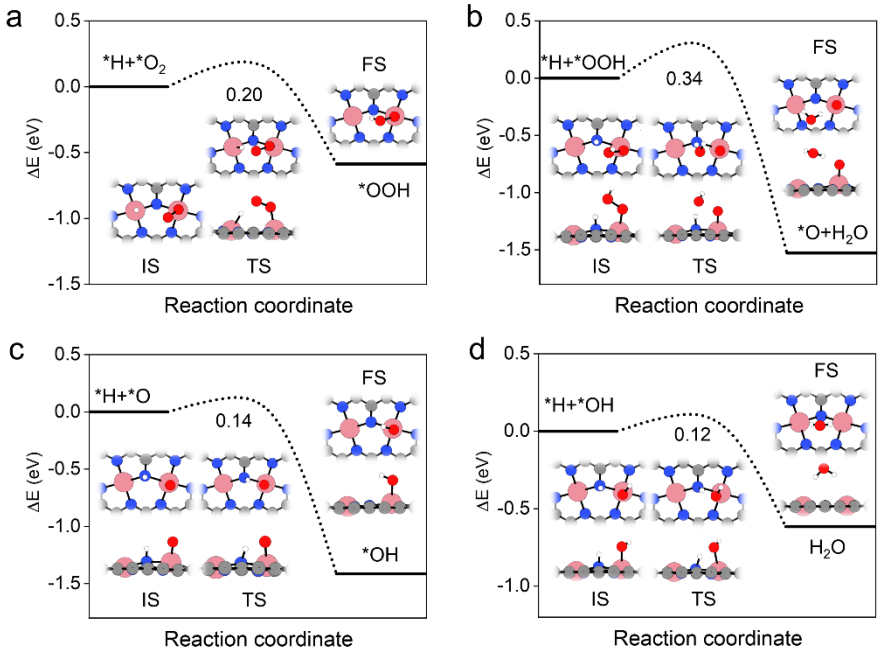

Supplementary Table 22. Calculated kinetic barriers for the **a** O_2 hydrogenation, **b** dissociation of *OOH, **c** *OH formation, and **d** second H_2O formation on Co-Co-Qv3. IS, TS, and FS denote the initial state, transition state and final state, respectively. The white, red, grey, blue, and pink spheres in the atomic models represent H, O, C, N, and Co atoms, respectively.

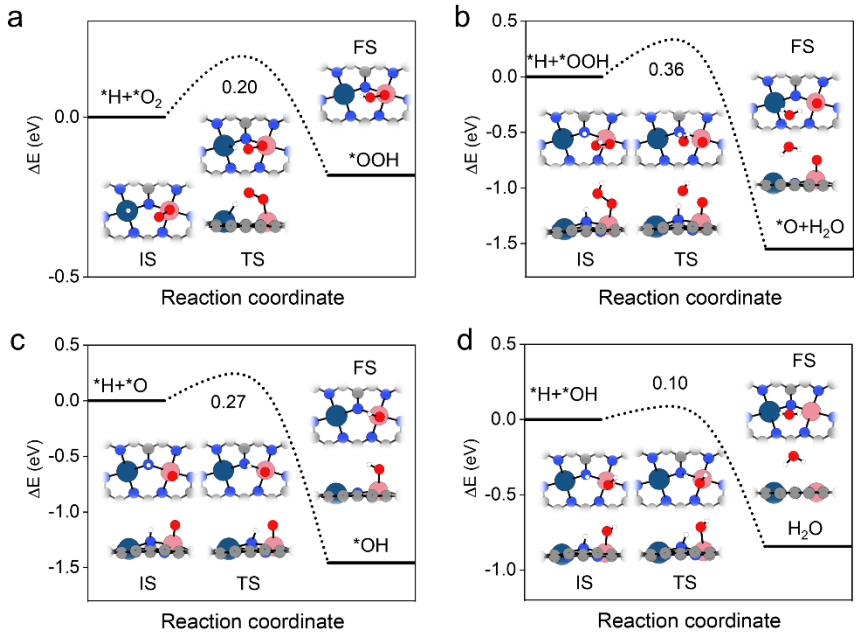

Supplementary Table 23. Calculated kinetic barriers for the **a** O_2 hydrogenation, **b** dissociation of *OOH, **c** *OH formation, and **d** second H_2O formation on Co-Ir-Qv3. IS, TS, and FS denote the initial state, transition state and final state, respectively. The white, red, grey, blue, pink, and dark blue spheres in the atomic models represent H, O, C, N, Co, and Ir atoms, respectively.

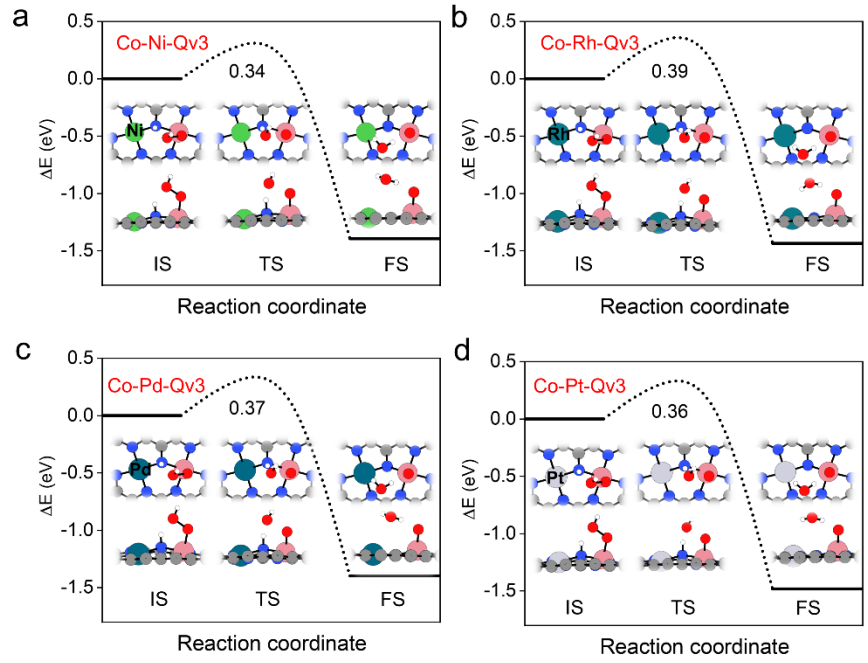

Supplementary Table 24. Calculated kinetic barriers for the dissociation of *OOH on **a** Co-Ni-Qv3, **b** Co-Rh-Qv3, **c** Co-Pd-Qv3, **d** Co-Pt-Qv3. IS, TS, and FS denote the initial state, transition state and final state, respectively. The white, red, grey, blue, and pink spheres in the atomic models represent H, O, C, N, and Co atoms, respectively.

Specific Comment R3-6: *Nowadays, new pathways for the oxygen reduction reaction (ORR) have been suggested, unlike the conventional one (O2 -> OOH -> O -> OH). If you apply a new pathway, are you confident that this trend can be maintained?*

Response: Many appreciations to the reviewer for this important comment. We fully agree that although the conventional association pathway (O_2 → *OOH → *O → *OH → H_2O) has been widely reported and studied, there are also some new ORR processes proposed, which further deepens our understanding of the reaction mechanism. The recent report has revealed that rather than the conventional association pathway, the dissociation pathways (O_2 → *O + *OH → *OH + *OH → *OH → H_2O) may be more favorable on dual-atom sites, such as Fe-Co-Qv2 (**D. Cheng** et al., *JACS Au* 2023, 3, 3031−3044). We also agree that a remarkable descriptor should have the ability to describe ORR activity across various reaction pathways, not only the conventional association pathway. Inspired by your kind reminder, we have additionally investigated the ORR activity on all X-Y sites mentioned in **Fig. 5b** via other three possible new dissociation pathways. **The results show that our developed descriptor remains a high prediction accuracy when new pathways are also considered.**

The schematic depiction of four association/dissociation pathways (Path-I~IV) has been supplemented in **Supplementary Fig. 21**. For each X-Y site, we selected the highest U_L(ORR) value among the four reaction pathways as the final U_L(ORR). We have revised all relevant data in **Fig. 5b**. It seems that the introduction of new dissociation pathways does not change the volcano-like structure-activity relationship constructed by our proposed descriptor ARSC. It is worth noting that this volcano-like correlation between ARSC and U_L(ORR) even be stronger. There are a total of 12 X-Y sites that favor the dissociation pathways, resulting in an increase in U_L(ORR) (as listed in **Supplementary Table 10)**. In line with the previous work, Fe-Co-Qv2 prefers Path-III and Path-IV with U_L(ORR) of 0.95 V instead of Path-I with U_L(ORR) of 0.73 V (**D. Cheng** et al., *JACS Au* 2023, 3, 3031−3044). These results further verify the reliability of our calculations.

The reason for why the trend can be maintained and only a subset of X-Y sites prefer new pathways can be explained as follows. As shown in **Supplementary Fig. 21**, the step of *OH desorption is included in all four association/dissociation pathways. In other words, for a X-Y site, if the step of *OH desorption is the PDS, the introduction of dissociative mechanisms will not optimize the ORR activity. We can conclude that the new dissociation pathways fail to further enhance the ORR activity on those dual-atom sites with stronger *OH adsorption, which are located at the left part of **Fig. 5b**, constituting a significant portion of the overall distribution. Moreover, if an X-Y site exhibits excessively weak adsorption of *OH and *OOH, the O_2 dissociation correspondingly becomes difficult. Therefore, for the X-Y site on the far right, such as Co-Y-Qv2, the new dissociation pathway remains less likely to occur. As a result, the X-Y sites that favor new pathways can only be concentrated near the volcano summit. With the introduction of new pathways, the limitations of a single conventional pathway can be rectified, leading to an improved accuracy of the descriptor.

We have provided the statement in the manuscript *page 13*:

Four ORR mechanisms are considered, including the conventional association and new dissociation pathways (Path-I~IV, **Supplementary Fig. 21**). Only 12 X-Y sites are found to favor the dissociation pathways (**Supplementary Table 10**), which are concentrated near the volcano summit.

We have updated the **Fig. 5b** in the manuscript:

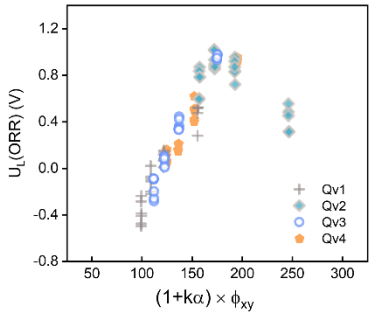

Fig. 5b. Volcano relationship between U_L(ORR) versus ARSC, defined as $(1 + k\alpha) \times \phi_{xy}$ on X-Y sites. X is Ru, Os, Fe, and Co; Y is Co, Ni, Rh, Pd, Ir, and Pt.

We have provided the **Supplementary Fig. 21** in the Supplementary Information:

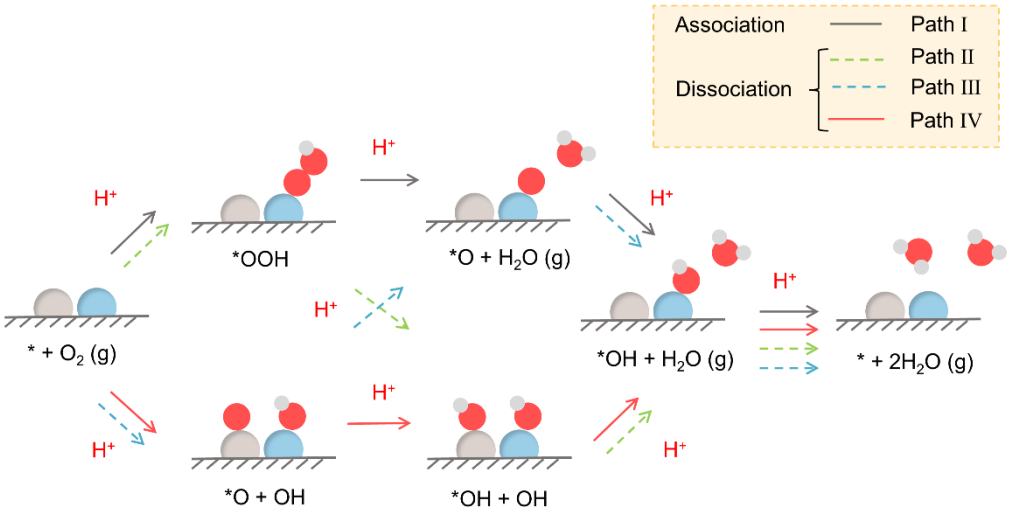

Supplementary Fig. 21. Schematic depiction of four association/dissociation pathways (Path-I~IV) for ORR on X-Y sites. Blue, X-metal; grey, Y-mteal; red, O; white, H.

We have provided the **Supplementary Table 10** in the Supplementary Information:

Supplementary Table 10. U_L(ORR) of X-Y sites that favor dissociation pathways.

X-Y site	U_L(ORR) Path-I	PDS Path-I	U_L(ORR) Path-I~IV	PDS Path-I~IV
Fe-Co-Qv2	0.73 V	$O_2 \rightarrow$ *OOH	0.95 V	*OH $\rightarrow H_2O$

Fe-Rh-Qv2	0.73 V	$O_2 \rightarrow$ *OOH	0.83 V	$O_2 \rightarrow$ *O + *OH
Ru-Ni-Qv2	0.82 V	$O_2 \rightarrow$ *OOH	0.93 V	*O + *OH → *OH + *OH
Ru-Pd-Qv2	0.86 V	$O_2 \rightarrow$ *OOH	1.02 V	*OH + *OH → *OH
Ru-Pt-Qv2	0.88 V	$O_2 \rightarrow$ *OOH	1.02 V	*OH + *OH → *OH
Os-Co-Qv2	0.75 V	*O → *OH	0.87 V	*OH → H_2O
Os-Ni-Qv2	0.42 V	*O → *OH	0.84 V	*OH + *OH → *OH
Os-Rh-Qv2	0.74 V	*O → *OH	0.78 V	*OH → H_2O
Os-Pd-Qv2	0.52 V	*O → *OH	0.60 V	*OH + *OH → *OH
Os-Ir-Qv2	0.76 V	*O → *OH	0.78 V	*OH → H_2O
Os-Pt-Qv2	0.55 V	*O → *OH	0.59 V	*OH + *OH → *OH
Co-Ir-Qv4	0.95 V	$O_2 \rightarrow$ *OOH	0.96 V	$O_2 \rightarrow$ *O + *OH

Specific Comment R3-7: *How can the solvation effect be included? If I haven't missed any information regarding this, there doesn't seem to be any discussion about the solvation effect. Could you please suggest the results when you include the solvation effect?*

Response: We are very grateful to the reviewers for your valuable reminder. To evaluate the effect of the solvation correction on the results, we have re-calculated the adsorption free energies as well as the limiting potentials of the dual-atom sites by adding the implicit model (Poisson-Boltzmann model). The implicit model is computationally inexpensive, which is widely adopted in high-throughput catalyst screening-related studies (**K. S. Kim** et al., *Energy Environ. Sci.* 2021, 14, 3455–3468; **X. Sun** et al., *Nat. Commun.* 2023, 14, 4449). By comprehensively investigating the solvation effect on X-X/X-Y sites for multiple reactions, **our calculations have indicated that solvation effects have little influence on the screening results for promising electrocatalyst candidates identified by our proposed descriptor,** in line with previous works (**T. Li** et al., *Adv. Funct. Mater.* 2022, 32, 2203439).

First, our previous work has verified that the solvation effect is negligible for NRR, which will bring a deviation of about 0.1 eV into the system, in line with previous reports (**J. Gong** et al., *Angew. Chem. Int. Ed.* 2023, 62, e202300122; **J. K. Nørskov** et al., *ChemSusChem* 2015, 8, 2180-2186; **Y. Jung** et al., *ACS Catal.* 2018, 8, 7517−7525). Therefore, we primarily focus on the solvation effect on ORR/OER/CRR.

To investigate the solvent effects on the adsorption free energies on different metals, we take the key intermediate *OH for ORR/OER as an example and compare the values of ΔG(*OH) on X-X sites with and without the implicit model, as displayed in **Supplementary Fig. 54a**. The results suggest that the introduction of the solvation correction is negligible for the activity trends between different metals since the slope of the linear fit approximates to 1. It is also worth noting that for the late transition metals, the solvation has a smaller impact on the adsorption free energies compared with the early transition metals. Since our calculations have indicated that most remarkable catalysts are concentrated among these late transition metals, this phenomenon confirms that solvent effects may be unlikely to alter our catalyst screening results for ORR/OER (**K. S. Kim** et al., *Energy Environ. Sci.* 2021, 14, 3455–3468).

To further evaluate the impact of the solvation correction on catalyst screening results, we comprehensively re-calculated U_L(ORR) with the implicit model via Path-I~IV on our selected potentially highly active X-Y sites (X = Ru, Os, Fe, Co, and Y = Co, Ni, Rh, Pd, Ir, Pt). As shown in **Supplementary Fig. 54b**, the activity trends of X-Y sites remain the same when the solvation corrections are introduced. One can see that the slope of the linear fit is 0.96 and most X-Y sites only exhibit a deviation within 0.1 V compared to the U_L(ORR) values without the implicit model. According to our calculation results corrected by the solvation effect, among these X-Y sites, the U_L(ORR) for Fe-Co-Qv2 is 0.93 V, in line with the 0.91 V reported by the previous work using the implicit model (**D. Cheng** et al., *JACS Au* 2023, 3, 3031−3044), which further suggests the reliability of our calculation results. In addition to *O- and *N-based adsorption, we also verified that the same results can be gained when U_L(CRR) with the implicit model on the potentially highly active X-Y sites (X = W, Mo, V, Re, Cr, Mn, Os, Ru, and Y = Fe, Co, Ir, Rh, Pd, Pt, Ni) were studied (**Supplementary Fig. 54c**).

We have provided the statement in the *Method* section:

Solvation effect

The solvation effect is taken into account via the implicit model (Poisson-Boltzmann model), which is implemented in VASPsol with a dielectric constant of 80[54]. For NRR, our previous work has verified that the solvation effect is negligible, which will bring a deviation of about 0.1 eV into the system, in line with multiple reports[13]. For ORR/OER, our calculations reveal that introduction of the solvation correction is negligible for the activity trends between different metals since the slope of the linear fit approximates to 1, especially for the late transition metals, confirming that solvent effects may be unlikely to alter our catalyst screening results for ORR/OER (**Supplementary Fig. 54a**). It is further verified by **Supplementary Fig. 54b** where most selected potentially highly active X-Y sites (X = Ru, Os, Fe, Co, and Y = Co, Ni, Rh, Pd, Ir, Pt) only exhibit a deviation within 0.1 V compared to the U_L(ORR) values without the implicit model. In addition to *O- and *N- based adsorption, we also found that the same results can be gained when U_L(CRR) with the implicit model on the potentially highly active X-Y sites (X = W, Mo, V, Re, Cr, Mn, Os, Ru, and Y = Fe, Co, Ir, Rh, Pd, Pt, Ni) were studied (**Supplementary Fig. 54c**). All these results reveal that solvation effects have little influence on the screening results for promising electrocatalyst candidates identified by our proposed descriptor.

We have provided the **Supplementary Fig. 54** in the Supplementary Information:

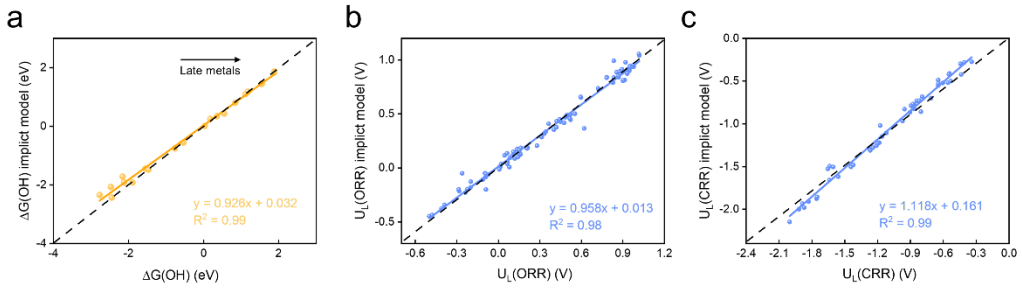

Supplementary Fig. 54. The comparison of **a** ΔG(*OH) on X-X sites, **b** U_L(ORR) on X-Y sites (X = Ru, Os, Fe, Co, and Y = Co, Ni, Rh, Pd, Ir, Pt), **c** U_L(CRR) on X-Y sites (X = W, Mo, V, Re, Cr, Mn, Os, Ru, and Y = Fe, Co, Ir, Rh, Pd, Pt, Ni) with and without the implicit model.

Specific Comment R3-8: *Previous high-throughput studies have already covered Co-Co dual atom catalysts. Could you please carefully compare your results with those of other studies? If there are discrepancies, kindly discuss the reasons for the differences.*

Response: Many appreciations to the reviewer for this crucial comment. Since Co-Co-Qv3 has been identified as optimal bifunctional oxygen catalysts in this work, we have summarized other high-throughput studies covering Co-Co dual-atom sites for effective bifunctional catalysts, as listed in **Supplementary Table 12**. Although these screenings considered Co-Co dual-atom sites, different coordination structures among them would lead to varying results. In previous works, Qv1 and Qv2 have been widely studied. The results show that Fe-M exhibit high activity for ORR while Co-M catalyze OER more effectively (*AIChE J.* 2024, e18459; *Appl. Surf. Sci* 2022, 605, 154714), in line with our calculations for Qv1 and Qv2. For Co-Co dual-atom sites, the overpotential of ORR and OER for Qv3 is 0.28 V and 0.29 V, respectively, superior to the results of high-throughput screening for Qv1 with different N-doping levels (*Adv. Funct. Mater.* 2022, 32, 2203439). This result suggests that Qv3-based DACs may be more suitable for bifunctional oxygen reactions. Due to our comprehensive high-throughput study including more metal-metal combinations and coordination structures, **multiple screening results for other Co-Co-related studies have been covered in our work, and more new DACs exhibiting higher bifunctional activity can be further identified in this work.** More importantly, **our work can quickly screen out multiple optimal DACs for various reactions and products simultaneously** based on our proposed universal intrinsic descriptor, which is what other high-throughput studies covering Co-Co sites has not yet achieved.

We have provided the statement in the manuscript *page 14*:

Compared with other high-throughput studies covering Co-Co dual-atom sites for effective bifunctional catalysts, multiple screening results have been covered in our work, and more new DACs exhibiting higher bifunctional activity can be further identified by ARSC (**Supplementary Table 12**). More importantly, our descriptor can quickly screen out multiple optimal DACs for various reactions and products

simultaneously, which is what other Co-Co-related high-throughput studies has not yet achieved.

We have provided the **Supplementary Table 12** in the Supplementary Information:

Supplementary Table 12. Comparison of other high-throughput studies covering Co-Co dual-atom sites for effective bifunctional catalysts. The highlighted DACs represent the identified promising bifunctional DACs.

Screened bifunctional DACs	Coordination structure	$M_1 \times M_2$	Descriptor	Ref.
Co-M-Qv3 Ru-M-Qv2, Fe-M-Qv2 for ORR Co-M-Qv1, Co-M-Qv4 for OER (M = Co, Ir, Ni, Pd, Pt, Rh) Cr-M, Mn-M for CRR (M = Fe, Co, Ir, Ni, Pd, Pt, Rh) Re-Re, Mo-Fe for NRR	Qv1, Qv2, Qv3, Qv4	20 × 20	Intrinsic	This work
Fe-M for ORR Co-M for OER	Qv1, Qv2	3 × 7	Electronic	AIChE J. 2024, e18459
Cu-Cu	C_2N	4 × 4	Energy-based	Carbon Lett. 2024, 34, 1367–1383
Pd-Pd, Pt-Pt, Pd-Pt	C_2N	30 MM 20 M_1M_2	Energy-based & electronic	J. Phys. Chem. Lett. 2023, 14, 1674−1683
Fe-M for ORR Co-Ni for OER	Qv2	3 × 3	Energy-based	Appl. Surf. Sci 2022, 605, 154714
Cu, Zn, Pd, Ag, Cd, Pt, Au-containing	Qv1 (C/N-doping)	27 × 27	Intrinsic	Adv. Funct. Mater. 2022, 32, 2203439
dual-CuN_3 for ORR dual-CoN_4 for OER	dual-TMN_3, dual-TMN_4	4 × 4	Energy-based	J. Mater. Chem. A, 2020, 8, 10193–10198
Fe-Ni, Fe-Co, Mn-Co	Qv1	10 × 3	Intrinsic	J. Phys. Chem. C 2020, 124, 27387−27395

Specific Comment R3-9: *If I understand correctly, there are some ad hoc or artificial parameters. For examples, the coefficient of alpha (k) is defined as one without any justification I wonder whether is there any physical or chemical reason to set this parameter like this or just numerically fit?*

Response: We are very grateful to the reviewers for this kind reminder. The parameter *k* is a result of numerically fit, which physically represents the weight of the coordination effect within the descriptor ARSC. A larger *k* value indicates that the coordination effect has a greater influence on activity. Here, *k* is exactly equal to 1 for ORR, and it can vary accordingly based on the characteristics of different reactions.

We have provided the statement in the manuscript *page 13*:

where *k* represents the coefficient for α, which physically represents the weight of the

coordination effect within ARSC. It is obtained by numerically fit and is exactly equal to 1 here.

Specific Comment R3-10: *Compared to other descriptors reported previously, how much superior are yours? For example, consider using other descriptors to extract candidates, synthesize and characterize them, and evaluate their electrochemical performance. Finally, compare the catalytic activity of your candidates with those obtained using other descriptors.*

Response: We thank the reviewer for this important suggestion. We fully agree that the electrochemical performance is a crucial factor when assessing the value of a descriptor, which will be discussed below. In addition, we believe that for a descriptor-based work, its insightful understanding of the structure-performance relationship, as well as its profound impact and promotion of subsequent related research, are equally extremely important. A superior descriptor would provide a comprehensive summary and deeper understand of the structure-performance relationship reported by previous works, especially for experimental works, and would provide universal guidance for subsequent catalyst design works with low cost instead of case by case. As a result, by comparing with other descriptor-related works for DACs, we will comprehensively evaluate the value of the descriptor reported by this work from six dimensions, namely practical utility, universality, physical meaning, developing method, experimental performance, and literature verification, respectively (**Supplementary Fig. 53**).

1. Practical utility and universality. In our response to R3-1, we have demonstrated that, like this work, an intrinsic descriptor comprehensively coupling the metal, synergistic, and coordination effects as well as multiple reactions are most perfectly suitable for guiding and accelerating the high-throughput screening of new effective electrocatalysts in terms of practical utility and universality (**Supplementary Fig. 52**). As shown in **Supplementary Table 19**, most papers still focus on traditional energy-based and electronic descriptors currently. However, those descriptors are case-by-case, unknown a priori and highly governed by the selected methodologies. That means if we want to evaluate a new material using those descriptors, time-consuming DFT calculations are needed for the adsorption energies or electronic structures first. And the conclusion may be different when we use different methodologies. As a result, the speed, cost, and scope of high-throughput screening will be greatly constrained. In addition, **among all intrinsic descriptors, only our work comprehensively considered multiple reactions with *O-, *N-, and *C-based intermediates** when constructing universal descriptors. The selectivity of DACs towards different reactions and products can also be showed with different scope of the descriptor values in this work. In our work, we have verified that, this descriptor, which is only built upon less than 4500 DFT calculations, successfully achieves the quick and low-cost prediction of effective DACs for various reactions and products instead of more than 50,000 high-throughput calculations. We have also verified that this descriptor can be expanded to other reactions and materials, bringing extensive insights to the subsequent design work of DACs. All these comparisons highlight the outstanding

practicality and universality of our descriptor.

2. Physical meaning and developing methods. Physical meaning is very significant for descriptors, as it can help us to understand the structure-performance relationship deeply. Nowadays, although we can directly correlate the catalytic performance with some intrinsic properties of active sites through various machine learning methods, extracting meaningful physical insights from these black-box models remains challenging due to their high degree of complexity (**S. Linic** et al., *Nat. Catal.* 2022, 5, 175−184). Interpretable machine learning methods have been developed to solve this problem, such as genetic programming and SISSO, which combines intrinsic properties into simper mathematical expressions as descriptors. However, the ability to display a descriptor in mathematical expressions does not necessarily mean it has a clear physical meaning, and there is always a tradeoff between simpleness and universality for interpretable descriptors. A descriptor that is simple, universal across different reactions, and physically insightful has not been reported yet due to limitations of existing interpretable ML methods. In response to this limitation, **we have constructed a new ML-based descriptor developing method, namely PFESS.** Correspondingly, the proposed descriptor shows a clear physical meaning, which quantifies the significant effect of the shape of frontier d-orbitals on catalytic performance at dual-atom sites. It is worth noting that most reported works still utilized the d-band model to explain the structure-activity relationship of DACs. However, given that the d-orbital of dual-atom sites is distinct and non-continuous, and the frontier orbitals have been reported to play the essential role in SACs (**R. Wu** et al., *Phys. Rev. Lett.* 2020, 125, 156001; **D. G. Vlachos** et al., *ACS Catal.* 2024, 14, 2, 886–896; **S. Caratzoulas** et al., *Angew. Chem. Int. Ed.* 2024, 63, e202311174), it becomes questionable whether the traditional d-band theory is still suitable for DACs. Our work has suggested that the d-orbitals of DACs lie between energy levels and energy bands, and **we innovatively combined the d-orbital theory and the frontier orbitals to comprehensively clarify the structure-activity relationship of DACs.** It proves a deeper physical insight of our proposed descriptor compared to other works. All these discussions illustrate the remarkable performance of this work in terms of physical meaning and developing methods.

3. Experimental performance and literature verification. According to our proposed descriptor, multiple DACs exhibiting remarkable catalytic performance have been quickly screened for different reactions. And we have selected Co-Co/Ir-Qv3 as a representative to investigate the experimental performance of descriptors. As shown in **Fig. 5i and Supplementary Tables 16 and 18**, we have verified the outstanding bifunctional electrochemical activity and stability of Co-Co/Ir-Qv3 for ORR/OER among a series of previous experimental works. We further compared the electrochemical activity of Co-Co/Ir-Qv3 with other effective DACs screened by reported descriptors. As displayed in **Supplementary Table 19**, descriptor-based works for graphene-derived dual-atom systems concentrate more on Qv1 or Qv2 as coordination structures. Since our descriptor exhibits higher universality which covers more coordination structures and metal-metal combinations, most screening results by

other descriptors have been included in our consideration. For example, as the effective DACs widely reported (*Phys. Rev. Applied* 2023, 19, 054094; *J. Catal.* 2021, 396, 215–223), Fe-Co-Qv2 still exhibits high activity for ORR but is not located at the peak of **Fig. 5b** in this work. In addition, **for some descriptor-based works, their identified high-active dual-atom sites have been synthesized, characterized, and tested by subsequent experimental works**, such as Co-Ni-Qv4, Fe-Ni-Qv1, Mn-Fe-Qv2, Fe-Ni-Qv2, Fe-Co-Qv2, and so on (**Supplementary Table 19**). As a result, **the comparison of electrochemical performance between ARSC and other descriptors can also be shown in Fig. 5h, where Co-Co/Ir-Qv3 are located at the peak of the volcano plot.** All these results indicate that the ideal DACs identified by our descriptors exhibit superior performance compared to other descriptors. In addition to the experimental performance, a more successful descriptor should be verified by multiple experimental literature. That means it can not only predict optimal catalysts reliably but also unify the different understandings of structure-performance relationship reported by previous experimental works. However, it seems that this comprehensive literature validation for a descriptor is challenging, which has been rarely reported. This work successfully correlates the structure-performance relationships of 28 experimental works, exhibiting an unprecedented depth of physical insight for dual-atom sites.

In summary, we have comprehensively demonstrated the outstanding performance of our proposed descriptors from six dimensions: practical utility, universality, physical meaning, developing method, experimental performance, and literature verification. The ARSC and corresponding PFESS method will undoubtedly bring a significant impact on subsequent catalyst design works. This work provides profound insights into the structure-activity relationship of DACs, paving the way for fast, low-cost, and high-throughput screening of effective catalysts with glass-box models.

We have provided the statement in the *Discussion* section:

Our descriptor exhibits superior performance from six dimensions: practical utility, universality, physical meaning, developing method, experimental performance, and literature verification (**Supplementary Table 19 and Supplementary Figs. 52 and 53**).

We have provided the **Supplementary Fig. 53** in the Supplementary Information:

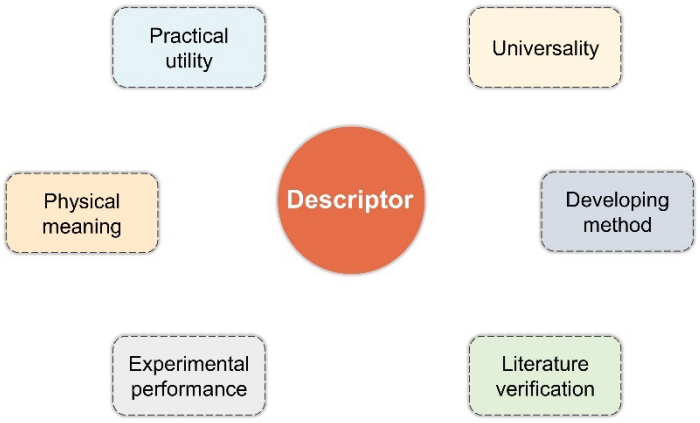

Supplementary Fig. 53. Schematic diagram of the evaluation for descriptors from six dimensions.

1. Practical utility and universality.

As shown in **Supplementary Fig. 52**, like this work, an intrinsic descriptor comprehensively coupling the metal, synergistic, and coordination effects as well as multiple reactions are most perfectly suitable for guiding and accelerating the high-throughput screening of new effective electrocatalysts in terms of practical utility and universality. While most papers still focus on traditional energy-based and electronic descriptors currently, which suffer from the high cost (**Supplementary Table 19**). More importantly, only our work comprehensively considered multiple reactions with *O-, *N-, and *C-based intermediates when constructing universal descriptors.

2. Physical meaning and developing methods.

Nowadays, a descriptor that is simple, universal across different reactions, and physically insightful has not been reported yet due to limitations of existing interpretable ML methods. In response to this limitation, we have constructed a new ML-based descriptor developing method, namely PFESS. Correspondingly, the proposed descriptor shows a clear physical meaning on the basis of high universality, where we innovatively combined the d-orbital theory and the frontier orbitals to comprehensively clarify the structure-activity relationship of DACs.

3. Experimental performance and literature verification.

As shown in **Fig. 5i and Supplementary Tables 16 and 18**, we have verified the outstanding bifunctional electrochemical activity and stability of Co-Co/Ir-Qv3 for ORR/OER among a series of previous experimental works. In addition, most screening results by other descriptors have been included in our consideration (**Supplementary Table 19**). For some descriptor-based works, their identified high-active dual-atom sites have been synthesized, characterized, and tested by subsequent experimental works. As a result, the comparison of electrochemical performance between ARSC and other descriptors can be shown in **Fig. 5h**, where Co-Co/Ir-Qv3 are located at the peak of the volcano plot. All these results indicate that the ideal

DACs identified by our descriptors exhibit superior performance compared to other descriptors. Moreover, a more successful descriptor should be verified by multiple experimental literature. However, it seems that this comprehensive literature validation for a descriptor is challenging, which has been rarely reported. This work successfully correlates the structure-performance relationships of 28 experimental works, unifying the different understandings of structure-performance relationship reported by previous experimental works. It exhibits an unprecedented depth of physical insight for dual-atom sites.

We have provided the **Supplementary Table 19** in the Supplementary Information:

Supplementary Table 19. Comparison of descriptors-based works for graphene-derived DAC system. The highlighted DACs represent that they have been experimentally synthesized, and the corresponding electrochemical performance have been shown in **Fig. 5h**.

Descriptor	Reaction	Coordination structure	$M_1 \times M_2$	Screened DACs	Ref.
Intrinsic	ORR/OER/ CRR/NRR	Qv1, Qv2, Qv3, Qv4	20 × 20	**Co-M-Qv3 for ORR/OER** Ru-M-Qv2, **Fe-M-Qv2 for ORR** Co-M-Qv1, Co-M-Qv4 for OER (M = Co, Ir, Ni, Pd, Pt, Rh) Cr-M, Mn-M for CRR (M = Fe, Co, Ir, Ni, Pd, Pt, Rh) Re-Re, Mo-Fe for NRR	This work
Intrinsic	ORR/OER	Qv1 (various N-doping level)	27 × 27	Cu, Zn, Pd, Ag, Cd, Pt, Au- containing	Adv. Funct. Mater. 2022, 32, 2203439
Intrinsic	ORR/OER	Qv1	10 × 3	**Fe-Ni, Fe-Co**, Mn-Co	J. Phys. Chem. C 2020, 124, 27387−27395
Electronic	ORR/OER	Qv1, Qv2	3 × 7	**Fe-M for ORR** Co-M for OER	AIChE J. 2024, e18459
Energy-based & electronic	ORR/OER	C_2N	30 MM 20 M_1M_2	Pd-Pd, Pt-Pt, Pd-Pt	J. Phys. Chem. Lett. 2023, 14, 1674−1683
Electronic	ORR	Qv2	10 × 10	ultrahigh-density Fe-Fe, Co-Co **low-density Fe-Co**	Phys. Rev. Applied 2023, 19, 054094
Electronic	ORR	Qv1, Qv2	6 × 6	**Fe-Mn-Qv2**, Fe-Fe-Qv2	J. Mater. Chem. A, 2022, 10, 9150–9160
Electronic	ORR	Qv1, Qv2,	6 × 6	**Fe-Co-Qv2**, Fe-Fe-	J. Catal.

		Qv4		Qv2	2021, 396, 215–223
Energy-based	ORR/OER	C_2N	4 × 4	Cu-Cu	Carbon Lett. 2024, 34, 1367–1383
Energy-based	ORR	Qv2, Qv3 (various N-doping level)	10 × 10	**Fe-Ni-Qv2 (6N), Mn-Fe-Qv2 (6N)**	Angew. Chem. Int. Ed. 2023, 62, e202311113
Energy-based	ORR/OER	Qv2	3 × 3	**Fe-M for ORR** Co-Ni for OER	Appl. Surf. Sci 2022, 605, 154714
Energy-based	ORR	Qv1	6 × 6	**Fe-Co**	J. Phys. Chem. C 2021, 125, 2334−2344
Energy-based	ORR/OER	dual-TMN_3, dual-TMN_4	4 × 4	dual-CuN_3 for ORR dual-CoN_4 for OER	J. Mater. Chem. A, 2020, 8, 10193–10198
Energy-based	ORR	Qv1	1 × 6	Ni-Zn	J. Phys. Chem. C 2020, 124, 11301−11307
Energy-based	ORR	Qv1, Qv4	4 × 4	Co-Pt-Qv4, **Co-Ni-Qv4**	ACS Catal. 2019, 9, 7660−7667

Specific Comment R3-11: *As a final comment, for the benefit of the data-driven society, I would suggest sharing the raw data and machine learning model on platforms like GitHub or Zendo. However, if you believe this information needs to remain confidential during the review or revision process, I recommend releasing the raw data and model after acceptance or publication.*

Response: We thank the reviewer for this kind reminder. We have included the atomic coordinates of the optimized model (CONTCARs), encompassing various configurations of DACs discussed in this work, as Supplementary Data 1. Additionally, the Python code developed for implementing the PFESS method and training universal descriptors has been released under the Apache 2.0 license. It can be accessed through our GitHub repository at https://github.com/TJU-ECAT-AI/PFESS. We are committed to enhancing the transparency of raw data further prior to publication.

REVIEWERS' COMMENTS

Reviewer #1 (Remarks to the Author):

I appreciate that the authors took my comments seriously, and feel that my concerns were adequately addressed.

Reviewer #2 (Remarks to the Author):

The authors have elaborately and systematically addressed my comments about:
1) ML descriptors considering the energy level of frontier orbitals.
2) Descriptions of the types of atomic radii and their performance in ML framework.
3) The DAC's stability and the DFT dataset's accuracy.
4) Further discussions on the screened-out Co-Co/Ir-Qv3.
5) and the other minor suggestions to improve the readability and reproducibility of this work.
Overall, this work is systematic and logically rigorous. The manuscript and SI are well prepared. I believe that this work related to Dual-atom catalysts, high-throughput catalyst screening, Machine learning, and electrocatalysis reactions is of interest to the readers of Nat. Commun. I have no further comments and recommend publication.

Reviewer #3 (Remarks to the Author):

The authors fully responded to my previous concerns. I now agree to the publication of this manuscript.

Reviewer #4 (Remarks to the Author):

I co-reviewed this manuscript with one of the reviewers who provided the listed reports. This is part of the Nature Communications initiative to facilitate training in peer review and to provide appropriate recognition for Early Career Researchers who co-review manuscripts.